

---

# DiSK: A Diffusion Model for Structured Knowledge

---

Ouail Kitouni<sup>\*1</sup> Niklas Nolte<sup>2</sup> James Hensman<sup>3</sup> Bhaskar Mitra<sup>3</sup>

## Abstract

Structured data presents unique challenges for standard language models due to their sequence bias. This paper introduces Diffusion Models of Structured Knowledge (DiSK) - a new architecture and training approach specialized for structured data. DiSK handles text, categorical, and continuous numerical data using a Gaussian mixture model approach. It employs diffusion training to model relationships between properties. Experiments demonstrate DiSK’s state-of-the-art performance on tabular data modeling, synthesis, and imputation across diverse domains. DiSK provides an effective inductive bias for generative modeling and manipulation of structured data. The proposed techniques could open the door to improved knowledge manipulation in future language models.

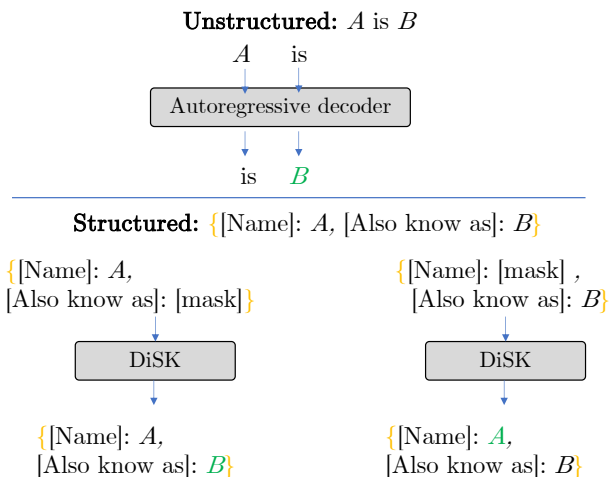


Figure 1. The next-token prediction objective retrieves information in only one direction, whereas DiSK models structured data with order-invariant training (see Section 3.2).

## 1. Introduction

How should we model structured data? One plausible approach is to type out the data into a structured format like JSON and train an autoregressive language model to make next-token predictions. However, such language models can struggle with knowledge manipulation tasks, as sequence modeling may not provide the right inductive bias to handle structured data (Allen-Zhu & Li, 2023).

For instance, it’s been shown that language models trained on the statement “A is B” fail to infer that “B is A” (Berglund et al., 2023). This limitation stems from the next-token prediction training objective, which only enables retrieval in one direction. Explicitly modeling entities (Figure 1) can help overcome this issue without prohibitive data augmentation (Zhu & Li, 2023; Allen-Zhu & Li, 2023). Instead of treating “A is B” as a next token prediction task, we can directly model the entity “A” by predicting its properties, such as “Also known as: B.” Modeling structured data in this way enables more explicit entity representations

<sup>\*</sup>Work done while interning at MSR. <sup>1</sup>Massachusetts Institute of Technology, IAFI <sup>2</sup>Meta AI <sup>3</sup>Microsoft Research. Correspondence to: Ouail Kitouni <kitouni@mit.edu>.

Preprint.

and improved knowledge manipulation and reasoning. As a step toward this goal, we propose Diffusion Models of Structured Knowledge (DiSK), which handle heterogeneous (categorical, numerical, text) structured data.

While tabular data may fit this paradigm, treating each row as an entity and each column as a property, tabular generative models are insufficient for highly sparse structured data or tables with missing values. DiSK handles both dense tabular data, where entities contain most properties, and sparse cases with varying properties per entity type. Our representation benefits tasks like imputing missing values and generating high-quality synthetic samples, which is becoming more important for training foundation models in various domains including language modeling (Li et al., 2023), mathematics (Trinh et al., 2024), and games with self-play data (Silver et al., 2017).

This paper makes the following contributions:

1. We propose adapting transformers for structured data by using hierarchical positional embeddings and a special numerical encoding without tokenization.
2. We develop a diffusion training objective that handles both discrete and continuous data, improving predictions on numerical quantities.
3. We achieve state-of-the-art performance on tabular data

modeling, synthesis, and imputation tasks.

In the remainder of the paper, we first survey related work on structured knowledge. We then present the DiSK architecture and training scheme. Finally, we empirically demonstrate the approach’s capabilities on diverse tabular reasoning benchmarks focusing on synthetic data generation and imputation. In these experiments, we first show how the structure inductive bias is advantageous compared to an unstructured language modeling baseline (LLaMA2-7B), then we show how DiSK improves upon a state-of-the-art method in tabular generative modeling in a task where entities have many missing properties, and finally, we show how the overall approach still achieves favorable performance even in the dense tabular case.

## 2. Related work

There is prior work on generative modeling of tabular data (Kotelnikov et al., 2023; Lee et al., 2023; Xu et al., 2019) that shares several characteristics with generative modeling of structured entities, insofar as a row in the tabular data can be considered as an entity and the corresponding heterogeneous column values as its set of properties. However, in structured entities, a property may also be composed of other datatypes—*e.g.*, a quantity is a composite of a numerical value and a unit of measurement (categorical type), and a date may be represented as a composite of three numerical values, *i.e.*, day, month, and year—which implies a richer hierarchical structure compared to a row in a typical tabular dataset. See Figure 2 for an illustration.

Previous work on generative models for tabular data has largely focused on the scenario where each row is a fixed-size vector of only numerical and categorical values that can be flattened into a simple feature vector. Unlike these previous works, we are interested in modeling richer datatypes, including text- and composite-datatypes. The framework we propose is flexible and extensible and, though outside the scope of this paper, can be used for large-scale pre-training on large and varied collections of knowledge bases.

Another relevant line of work is Knowledge Base (KB) modeling which is often viewed as a link prediction problem, where the knowledge base is represented as a collection of factual triples (head, relation, tail) (Bordes et al., 2013; Lin et al., 2015; Sun et al., 2018; Schlichtkrull et al., 2018; Nathani et al., 2019). This often necessitates a high-quality subset of triples, and conventional models may struggle to generalize to generating facts with entirely new entity tails. In this work, we take a more direct approach and model the knowledge base as a collection of entities, framing knowledge modeling as a masked property prediction task over incomplete entity representations. The proposed training procedure and model architecture are designed to

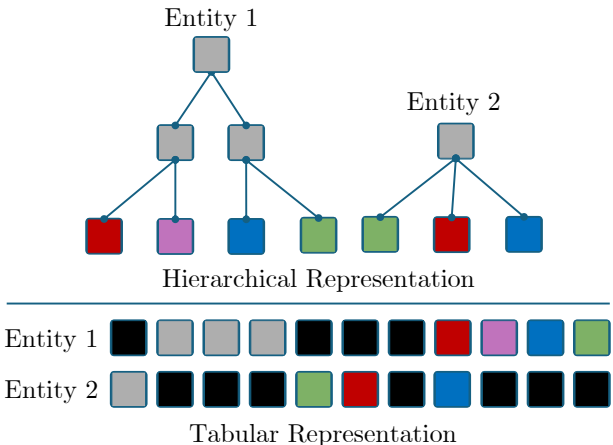


Figure 2. Hierarchical representations of entities can model rich relationships that can be difficult to capture with dense tabular representations, which can be prohibitive for sparse KBs. Black squares correspond to non-existing values, making the table sparse.

capture interdependence between properties. Furthermore, our new evaluation scheme focuses on capabilities relevant to knowledge-intensive tasks. For instance, instead of deciding whether links are factual or not, this approach focuses on entity completion from prior associations. Our KB model does not simply learn to assess the validity of a particular triplet; it learns algorithms to derive an entity’s properties.

## 3. Generative Modeling of Structured Entities

A common approach in the literature for generating new facts is to evaluate the validity of triples using link prediction models. Instead, we take a generative perspective on knowledge base modeling. In this section, we describe the training procedure of a generative model with (fixed-mask) masked modeling. We then show a simple loss modification to formulate the problem as an absorbing continuous-time diffusion over discrete states. This formulation allows samples to be more consistent and of higher quality by smoothing the generative process over small steps in the number of properties unmasked per iteration.

### 3.1. Masked Modeling

A naive approach to training our entity completion model, parameterized by  $\theta$ , is to directly predict hidden properties based on a subset of available properties using a fixed mask, similar to Devlin et al. (2019). Consider an entity  $x \sim p(x)$  where each dimension corresponds to a property. At each training step, the model is given a collection of properties associated with the entity,  $\tilde{x}$ . Some property values are replaced with a special mask token. The model then predicts the true values of the masked properties conditioned on the

visible properties

$$\mathcal{L}_{CT} = \mathbb{E} \left[ \sum_{d|\tilde{x}^d \text{ is masked}} -\log p^\theta(x^d | \tilde{\mathbf{x}}) \right], \quad (1)$$

which amounts to a per-property reconstruction loss (e.g., using cross-entropy or mean squared error). At inference time, the model is used exactly in the same fashion. A collection of properties is given and the model predicts all remaining properties in a single step.

This approach is not necessarily optimal in terms of the quality of generated samples. Single-step models can be inferior to traditional left-to-right autoregressive models, so it is natural to expect improved quality of generated samples if the model is allowed to fill in the missing properties autoregressively (Ghazvininejad et al., 2019). At the cost of more computation, the diffusion approach we will formalize in the next section solves this issue (see Appendices B.1.2, for an intuitive example, and B.1.1 for a full ablation).

### 3.2. A Formulation of Diffusion over Heterogenous Data

We now explore a diffusion modeling approach based on Discrete Denoising Diffusion Probabilistic Models (D3PM) (Austin et al., 2021), specifically continuous-time discrete-state diffusion (Campbell et al., 2022) with an absorbing state. In the following, we will define a diffusion paradigm that can be seen as an autoregressive extension of the masked modeling approach. In Figure 3, we see how both setups can be used to sample new entities.

Our proposed diffusion process can be summarized as (1) For an entity  $\mathbf{x}_0 \sim p(\mathbf{x}_0)$  with  $D$  dimensions, individual properties randomly flow into the absorbing masked state. At the end of this process, all properties are masked. (2) The reverse process, which is completely defined by the forward process but is generally intractable, is modeled via a parameterized conditional distribution, at step  $t$ ,  $p^\theta(\mathbf{x}_{t-1}|\mathbf{x}_t)$  as the random de-masking of individual properties,  $x^d$ . The objective is to maximize the log-likelihood of the data under this reverse conditional.

**Forward Process** The noising process randomly masks an entity’s properties at a sampled rate. Surprisingly, the objective reduces to the standard reconstruction loss weighted by masking amount. The complete derivation is available in Appendix A.2; this section outlines the initial steps. Consider the forward process  $q(\mathbf{x}_t|\mathbf{x}_{t-1})$  from  $p(\mathbf{x}_0)$ , the data distribution, towards an easy-to-sample reference distribution  $q(\mathbf{x})$  with all dimensions (properties) in the masked state. We apply a continuous-time diffusion to dimension  $d$  of  $\mathbf{x}_0$  with a transition rate matrix

$$R_t^d = \begin{bmatrix} 0 & 0 & 0 \\ -\beta(t) & \beta(t) & 0 \\ -\beta(t) & 0 & \beta(t) \end{bmatrix},$$

where, for illustration purposes, we used a discrete distribution with 3 states and reserved the state 0 for the mask state. Each state flows into the absorbing mask state with the same rate  $\beta(t)$ . Solving Kolmogorov’s equations, reveals the marginal distribution for the state at time  $t$  conditioned on the initial state is given by  $\mathbf{x}_0^T P_t$  (using a slight abuse of notation to handle all dimensions simultaneously) where

$$P_t^d = \exp \int_0^t R_s^d ds = \begin{bmatrix} 1 & 0 & 0 \\ 1 - e^{-\gamma(t)} & e^{-\gamma(t)} & 0 \\ 1 - e^{-\gamma(t)} & 0 & e^{-\gamma(t)} \end{bmatrix}, \quad (2)$$

with  $\gamma(t) = \int_0^t \beta(s) ds$ . At time  $t$ , property  $d$  jumps into a masking state with probability  $1 - e^{-\gamma(t)}$ , while masked properties remain absorbed. We set  $\beta(t)$  such that at time  $t = 1$ , all properties are masked (i.e.,  $\gamma(1) = \infty$ ). The specific  $\beta(t)$  is irrelevant as we can integrate across the masking probability instead of time, similar to integrating across the signal-to-noise ratio (SNR) in Kingma et al. (2021) for Gaussian diffusion models. Though the forward process is independent for each dimension, it is useful to denote the joint rate over properties

$$R_t(\mathbf{x}, \tilde{\mathbf{x}}) = \sum_{d=1}^D \delta(\mathbf{x}^{-d}, \tilde{\mathbf{x}}^{-d}) R_t^d(x^d, \tilde{x}^d), \quad (3)$$

where  $-d$  indexes is a vector of all properties from 1 to  $D$  except property  $d$ . Here, the Kronecker delta  $\delta$  is used to specify that there is no change from one vector to another unless exactly one property,  $d$ , changes, in which case the rate is given by the rate matrix for that property. The total rate of change across all properties is then given by

$$Z_t(\mathbf{x}) = \sum_{\mathbf{x} \neq \tilde{\mathbf{x}}} R_t(\mathbf{x}, \tilde{\mathbf{x}}) = \beta(t)(D - N_t), \quad (4)$$

where  $N_t$  is the number of masked properties at time  $t$ . It is also useful to write the probability of transitioning from state  $\mathbf{x}$  to  $\tilde{\mathbf{x}}$  at time  $t$  as  $r_t(\tilde{\mathbf{x}}|\mathbf{x}) = (1 - \delta(\mathbf{x}, \tilde{\mathbf{x}})) R_t(\mathbf{x}, \tilde{\mathbf{x}}) / Z_t(\mathbf{x})$ . We can also define the empirical masking rate  $\hat{\pi} = N_t / D$ . These expressions will be useful in deriving the likelihood bound in Proposition 3.1 (see Appendix A for more details).

#### A simple simulation of the backward diffusion process

With our forward process defined, we focus on the backward process. We know from our choice of the forward process that at time  $t = 1$  the state will be all masks with probability 1. In the reverse process, Equation 8 (see Appendix A.1) tells us that once a property has been de-masked, it will stay de-masked until  $t = 0$ . Masked properties transition to de-masked states at a rate proportional to the model’s prediction given the current state. Because all the properties flow at the same rate, the order in which the properties are de-masked is random, irrespective of the model. As we approach  $t = 0$ , the rate approaches infinity, fully de-masking all properties by  $t = 0$ .

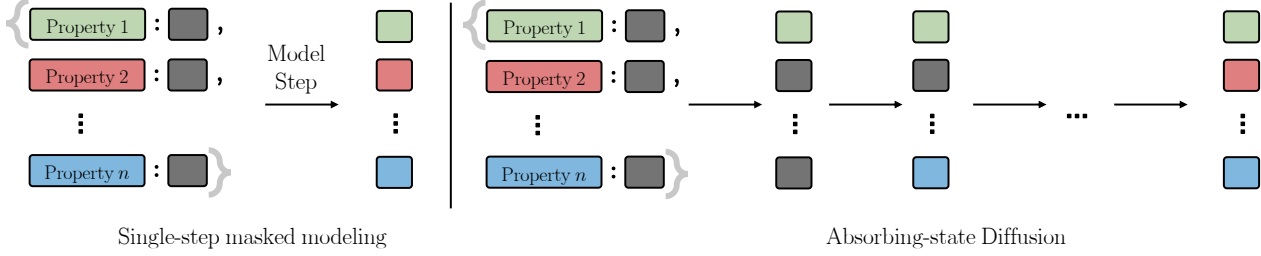


Figure 3. Generating samples with keys “property  $j$ ” using masked modeling in one step (left) and autoregressively (right), in which case property values are unmasked in random order.

A simple algorithm can implement the reverse diffusion process as follows: First, initialize with a sequence comprising entirely masked states. Then, randomly select a masked property and predict its new state using the neural network, conditioned on the current states of all properties. Replace the selected property’s masked state with its newly predicted state. Repeat this process, picking randomly masked properties and predicting their unmasked states until no masked states remain. While this simulation disregards event timing, that omission is inconsequential for our purposes. Unmasking is not restricted to removing one mask at a time; instead, we can employ multiple leaps ( $> 1$ ) in every step (Campbell et al., 2022). When the leap count is equal to the number of properties, the reverse diffusion process is equivalent to the generative step from the masked modeling procedure, and we simply predict all properties at once. Although this approach may offer computational advantages, it could also weaken the correlations that maintain the samples’ consistency (see Figures 6 and 7 as well as the ablation study in Appendix B.1).

**Likelihood bound** The choice of absorbing state kernel yields a surprisingly simple likelihood bound, which can be written as a denoising loss weighted by the amount of masking noise.

**Proposition 3.1.** *For the reverse diffusion from the fully masked stationary distribution towards  $p(\mathbf{x}_0)$ , an upper bound on the model negative loglikelihood  $\mathbb{E}_{p(x)}[-\log p_0^\theta(x)]$  can be given by*

$$\mathcal{L}_{CT} = \mathbb{E}_{\pi \sim \mathcal{U}(0,1), \tilde{\mathbf{x}} \sim \psi(\tilde{\mathbf{x}})} \left[ C(\pi) \sum_{d|\tilde{\mathbf{x}}^d=0} -\log p_{0|t}^\theta(x_0^d | \tilde{\mathbf{x}}) \right], \quad (5)$$

where  $\psi(\tilde{\mathbf{x}}) = \sum_{\mathbf{x}} q_t(\mathbf{x}) r_t(\tilde{\mathbf{x}}|\mathbf{x})$  and  $C(\pi) = D \frac{1-\hat{\pi}}{1-\pi} \frac{1}{N_t+1}$ .

A full proof is available in Appendix A. The terms in green (under the expectation) are a direct implementation of the simulation process described in detail in Appendix A.2, the term in blue (the prefactor to the sum) is a simple rescaling factor, and the term in red (the sum) is the usual reconstruction loss but with a random masking rate.

**A Continuous Relaxation of Discrete State Diffusion** So far, we have only discussed discrete-state diffusion, valid for categorical properties. Here, we turn our attention to numerical properties. To predict numerical values to a high degree of precision, we can choose a discretization with a large but finite number of bins and employ all the machinery we developed up to this point. The full softmax can become quite expensive to evaluate in this case. Though there are several ways to alleviate this issue, such as hierarchical softmax (Morin & Bengio, 2005) or various contrastive alternatives (Oord et al., 2018; Sohn, 2016; Oh Song et al., 2016; Schroff et al., 2015), we will instead approximate the softmax when the number of bins (classes) tends to infinity.

We will end up using a Gaussian Mixture Model (GMM) for numerical properties. But first, to develop some intuition, we will explore a simplified approach where we assume we only want to model Gaussian numerical properties. A reasonable categorical model of continuous values captures ordinal properties and approaches Gaussian uncertainty in the limit of a large number of classes. Suppose the “correct” target value is  $x$ , we can take the discrete distribution  $P(b_i) \propto \exp(-||x - b_i||^2)$ , where  $b_i$  is the bin-center of the  $i$ -th bin. In this case, we can write out the cross-entropy loss over bins, assuming  $x$  is in the  $i$ -th bin, as follows  $-\log P(b_i) = -\log \text{softmax}(-(\mathbf{b} - x\mathbf{1})^2)_i$ , which is simply  $-\log \exp(-(b_i - x)^2)$ , ignoring the normalization, we can use squared error  $(b_i - x)^2$  as a de-masking loss. In this setup, optimizing the cross-entropy over a large number of bins amounts to optimizing the center of the target bin using the mean-squared-error (MSE), avoiding a potentially prohibitive computation. With our loss function and generative procedure defined, we can move our focus to the neural architecture we will employ.

## 4. DiSK Architecture

This section describes the DiSK model architecture, with Figure 4 showing a high-level overview. DiSK takes an entity with an arbitrary number of properties of any type (any of which can be missing or “masked”). The property keys are used to generate semantic hierarchical encodings,

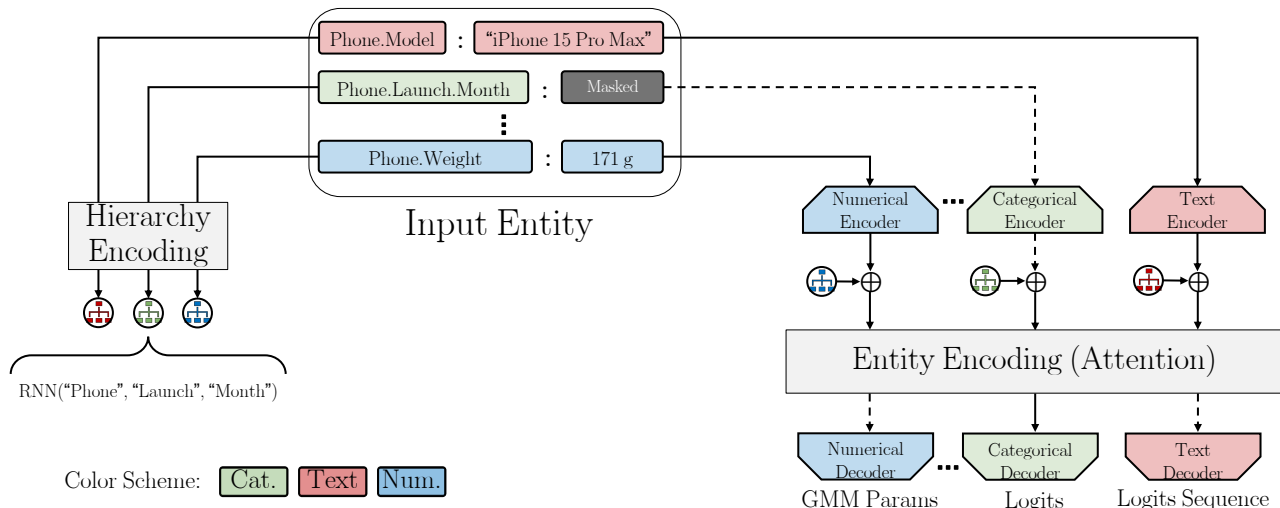


Figure 4. The DiSK architecture. Keys from the input entity are used by an RNN to generate hierarchical encodings (left). They are then added to encoded values (right) the result is processed by an encoder and type-specific decoders output logits and GMM parameters. Dashed lines are not computed *i.e.* masked values are not encoded and unmasked values are not predicted.

and property values are passed to an encoder for the appropriate type. The outputs of both encoding steps are added together. For missing or masked properties, values are not encoded and only their hierarchical encodings are used. A transformer module aggregates information across properties and each element gets decoded into the appropriate probabilistic parameters we would later sample from *i.e.*, GMM means, variances, and weights for numerical properties and logits for text and categorical properties. Only masked properties are decoded, and the loss is evaluated on them. We will now provide more details on each step (see Appendix C for technical details).

**Hierarchical positional encoding** Our goal is for the model to understand entities’ properties semantically. The hierarchical encodings are generated using a sequence model over the keys; in our setup, we use a simple RNN over the path to the node of interest (see Figures 4 and 9). Alternatively, language model representations could be leveraged, reading off the hierarchical encoding from a special token like BERT’s [CLS] token (Devlin et al., 2019).

**Encoding** Each property value will first be embedded. Embedding schemes differ for each type of input, in this case, text, categorical and numerical. Categorical variables, just like text tokens, are one-hot encoded, as is standard in language modeling. Numerical values need to be treated differently in order to preserve their numeracy properties. DICE (Sundararaman et al., 2020) embeddings or the standard sinusoidal embeddings (Vaswani et al., 2017) with learnable frequencies are good options. Though DICE embeddings preserve magnitude and order by construction, we could not find conclusive evidence for the superiority of

either approach (see ablations in Appendix B.2). Each property value passes through an encoder module tailored to that property type. This can be achieved either via conditioning on the property itself (through the hierarchy positional encoding, for instance) or via disjoint encoders for each property. We opt for the latter in our experiments.

The encoder architecture suits the input modality, mapping inputs to fixed-dimensional vector representations. We use MLPs with residual connections for categorical and numerical properties and we extract the first token representation from a Transformer encoder for text fields. Note that we can also use pre-trained language models as encoders for text properties but that is beyond our scope. These encoders map heterogeneous properties into a shared entity latent space. Their role is to transform arbitrary input types into a common representation format.

**Entity encoding and decoding to property values** After encoded properties have been augmented with positional encodings, multiple Transformer encoder layers process the properties. Masked elements are not attended to. With full entity context, property encodings are decoded via specialized decoders. Again we have the option of tying them (with conditioning), but we choose to use disjoint modules. Decoders output probabilistic parameters - logits for categorical/text, and GMM parameters ( $\mu$ ,  $\sigma$ , weight) for numerical values. These parameters define the distributions we can sample from in the reverse process. For text properties, we use a transformer decoder to generate a sequence of tokens conditioned on the property encoding. Such bottlenecks were previously explored in Mu et al. (2023) and shown to give good performance.

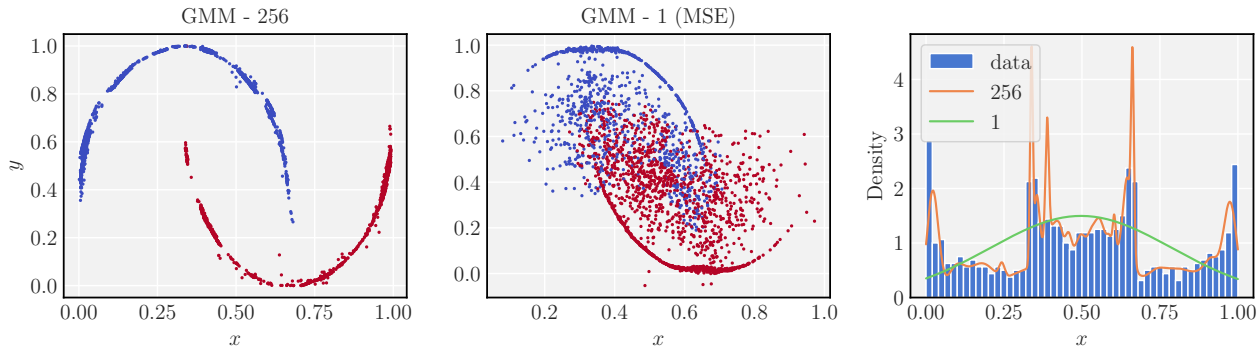


Figure 5. Generated samples using a DiSK with GMM likelihood. The GMM uses 256 components (left) or 1 component (middle) which is equivalent to MSE when we fix the variance to unity. (right) A histogram of the data with the DiSK learned marginals.

**Revisiting Numerical Properties** In section 3.2, we approximated the softmax computation for numerical quantities using MSE. However, this results in reduced model expressivity and inability to capture multi-modal distributions of properties. A Gaussian Mixture Model (GMM) with additional components can address this. Figure 5 presents a toy DiSK model trained on the two moons dataset, treating  $x$  and  $y$  as numerical and class as a categorical property. Contrary to the MSE-trained model, the GMM-trained model effectively captures the multiple modes of  $x$ ’s marginal distribution.

## 5. Experiments

**The Efficiency of Structure** First, we show experiments using the Kaggle GSMArena dataset (Appendix F). We show that, when dealing with structured data (such as knowledge bases), the structured DiSK architecture outperforms baselines consisting of unstructured text decoder-only models. We perform the experiment using both a fine-tuned LLaMA2-7B model (Touvron et al., 2023) and a small decoder-only model trained from scratch. In particular, it is evident that at a lower parameter count, the structured inductive bias provides gains over the unstructured baseline at much larger scales. Furthermore, we show that we get favorable performance compared to Gradient-Boosted Decision Trees, which offer state-of-the-art performance on tabular data. The GBDTs are trained to predict a single property based on all others, offering a strong baseline. Unlike DiSK, GBDTs do not handle missing data naturally, which can explain the performance gap (see F for more training details).

All models use a 80-20 train-test split. The decoder-only architectures (pre-trained and randomly initialized) use next-token prediction. LLaMA inputs are JSON-formatted string representations, with properties (key-value pairs) permuted 10 times before tokenization to augment the training set. Without this augmentation, causal models achieve worse

performance because of difficulties in knowledge manipulation (Zhu & Li, 2023). To evaluate predictions on a particular property, we prompt the model with all other property keys and values followed by the key of the property we aim to predict. The model must output the property value and a closing brace to form valid JSON. See additional details in Appendix F.1. Note that this evaluation heavily favors the autoregressive models. These choices aim to present a challenging “best effort” scenario, establishing a difficult benchmark to surpass. Naturally, DiSK is capable of making predictions using a much smaller number of properties. Figure 12 shows the metrics as a function of the proportion of properties given.

The unstructured decoder-only architectures demonstrate impressive prediction capabilities, especially LLaMA, though pretraining may enable data leakage. We provide a zero-shot LLaMA experiment to gauge this effect. However, those decoders lack critical inductive biases for structured data like the ordinality of numerical properties. In contrast, DiSK incorporates these properties, improving performance on structured data versus LLaMA, as Table 1 shows. This highlights the importance of embedding structure-aware inductive biases, even at massive scale. While decoder-only models can memorize statistical regularities, their lack of inherent constraints results in exploding errors without augmentation. They also struggle to output valid, parseable entities, particularly at small scales. DiSK’s structured formulation prevents these issues by design.

**Nuclear Physics Predictions** Many scientific applications lack large-scale data due to the difficulty of taking measurements, the rarity of the events measured, or the prohibitive cost of obtaining more data. We will explore the benefits of using a KB generative model to learn from limited data. Nuclear properties are a good example, and developing accurate models for them can have a large impact on many subfields of physics, such as nuclear (astro)physics, including  $r$ -process nucleosynthesis (Burbidge et al., 1957), the

Table 1. Comparison of causal decoder-transformer and structured generative modeling for property prediction. Numerical properties (above line) use RMS error. Categoricals (below line) use error rate (1 - accuracy). “model” is a text field and uses word-based intersection over union (IoU) since tokenizers differ. To ensure that smaller values are better for all fields, we use 1 - IoU for text. Parsing error rate measures invalid JSON string predictions.

Field	DiSK	Decoder no pretrain	LLaMA2- 7B	GBDT Baseline
weight	<b>20.8</b> $\pm$ 0.5	71.9	24.2	25 $\pm$ 1
height	<b>5.7</b> $\pm$ 0.2	79.6	6.4	6.2 $\pm$ 0.2
depth	<b>1.67</b> $\pm$ 0.05	3.90	1.82	<b>1.65</b> $\pm$ 0.04
width	<b>3.5</b> $\pm$ 0.3	42.7	4.110	<b>3.8</b> $\pm$ 0.2
display-size	<b>0.64</b> $\pm$ 0.02	7.47	0.707	1.08 $\pm$ 0.05
battery	<b>0.233</b> $\pm$ 0.008	6.99	0.257	0.304 $\pm$ 0.007
launch.day	11 $\pm$ 1	30.9	11.27	<b>8.7</b> $\pm$ 0.2
launch.month	3.4 $\pm$ 0.02	4.79	5.11	<b>3.281</b> $\pm$ 0.005
launch.year	<b>1.25</b> $\pm$ 0.06	947	<b>1.22</b>	1.42 $\pm$ 0.02
oem	<b>0.181</b> $\pm$ 0.005	0.484	0.231	0.4 $\pm$ 0.02
network-edge	0.221 $\pm$ 0.005	0.371	<b>0.217</b>	0.75 $\pm$ 0.01
model	<b>0.881</b> $\pm$ 0.004	0.900	<b>0.878</b>	–
parsing err. rate	0%	3.6%	3.9%	0%
num. params	24.8M	30.7M	7B	–

nuclear neutron skin and its consequences for the structure of neutron stars (Brown, 2000; Horowitz & Piekarewicz, 2001; Gandolfi et al., 2012), the exploration of the boundaries of the nuclear landscape (Erler et al., 2012), etc.

Here we tackle the knowledge completion task, on a nuclear physics dataset, comprising 3254 nuclei. The features that we predict here are categorical and numerical in nature, detailed in Appendix E. An important property of this dataset is that it has many missing features and can be a testbed for how well our model handles sparse data. We explicitly exclude two prominent features, proton and neutron separation energy, because they cause data leakage across train and validation dataset for the arguably most important property, the binding energy. To our knowledge, no single model predicts the diverse physical properties we consider. However, specialized binding energy models provide reasonable baselines, with errors from 140 keV to several MeV using hand-engineered inputs and considerable domain knowledge (Gao et al., 2021; Wang et al., 2014; Zeng et al., 2022; Wang et al.; Wu et al., 2022).

We provide a Tabular Denoising Diffusion Model (TDDPM) baseline from Kotelnikov et al. (2023), which is specifically designed to work on tabular data and only handles categorical and numerical features (omitting text, for instance). We evaluate models using 5 initialization seeds. See Appendix E.1 for more details. DiSK has favorable performance on most properties (Table 2), and because TDDPM does not handle missing data naturally, its performance on the Stability property is not much better than the constant baseline. Our native handling of sparse data and missing

Table 2. Performance on the Nuclear Physics dataset. RMS values for numerical values above the line and errors for categorical features below. Properties without a unit specification have no units. Volume, Surface, Symmetry and Coulomb are unitless quantities related to proton and neutron numbers. The Optimal Constant Baseline uses the mode for categorical and mean for numerical properties.

Field	DiSK	TDDPM	Optimal Const.	GBDT Baseline
$E_b$ [keV]	<b>370</b> $\pm$ 40	1700 $\pm$ 70	5570	640 $\pm$ 40
Radius [fm]	<b>0.011</b> $\pm$ 0.001	0.445 $\pm$ 0.008	0.717	0.169 $\pm$ 0.009
$t_{1/2}$ [logsec]	<b>1.51</b> $\pm$ 0.01	2.63 $\pm$ 0.02	3.63	1.72 $\pm$ 0.09
Spin	1.2 $\pm$ 0.1	1.78 $\pm$ 0.02	1.74	<b>1.02</b> $\pm$ 0.01
Abundance	<b>10.8</b> $\pm$ 0.1	13.7 $\pm$ 0.1	14.8	<b>10</b> $\pm$ 1
$Q_\alpha$ [keV]	<b>360</b> $\pm$ 50	1330 $\pm$ 30	6592	1290 $\pm$ 40
$Q_{\beta^-}$ [keV]	<b>310</b> $\pm$ 20	2350 $\pm$ 80	7781	1790 $\pm$ 80
$Q_{\beta^- + n}$ [keV]	<b>440</b> $\pm$ 80	2800 $\pm$ 200	10558	2300 $\pm$ 100
$Q_{EC}$ [keV]	<b>520</b> $\pm$ 40	2340 $\pm$ 80	7643	1900 $\pm$ 100
$\beta_2$ [barns]	0.93 $\pm$ 0.02	1.26 $\pm$ 0.02	1.36	<b>0.43</b> $\pm$ 0.02
Volume	<b>0.8</b> $\pm$ 0.1	3 $\pm$ 1	66.49	<b>0.88</b> $\pm$ 0.05
Surface	0.21 $\pm$ 0.02	0.5 $\pm$ 0.1	8.763	<b>0.127</b> $\pm$ 0.007
Symmetry	<b>0.218</b> $\pm$ 0.002	0.28 $\pm$ 0.04	4.137	0.35 $\pm$ 0.02
Coulomb	<b>5.3</b> $\pm$ 0.6	6 $\pm$ 1	482.8	11 $\pm$ 0.6
Stability	0.01 $\pm$ 0.001	0.088 $\pm$ 0.005	0.076	<b>0.004</b> $\pm$ 0.001
Parity	<b>0.047</b> $\pm$ 0.003	0.36 $\pm$ 0.01	0.68	0.077 $\pm$ 0.007

values can explain much of the performance gap observed here.

Finally, the probabilistic predictions enable reporting modeling uncertainties, which is critical for physics. We can use the denoising model to estimate various joint and conditional probabilities. Figure 11 in the appendix shows example binding energy uncertainty estimates.

**Generative Modeling for Tabular Data** We evaluate the quality of DiSK generated samples via the performance of a downstream model trained on the synthetic data. Following Kotelnikov et al. (2023), we trained and tuned a GBDT to perform the downstream task, which can be either regression (evaluated with  $R^2$ ) or classification (evaluated with  $F_1$  score). Across 15 datasets, detailed in Appendix D, we generate 5 synthetic samples and train 10 GBDTs with different seeds. Then we evaluate the performance on a held-out test set from the original data. We compare performance against various generative models specializing in structured tabular data such as TabDDPM (Kotelnikov et al., 2023), CTAB-GAN (Zhao et al., 2021), TVAE (Xu et al., 2019) as well as an interpolation technique, SMOTE (Chawla et al., 2002), as a sanity check. Evaluation metrics as well as preprocessing are taken from (Kotelnikov et al., 2023). In a majority of cases, DiSK offers favorable performance, as shown in Table 3, but falls somewhat short on, notably, the largest dataset here: FB-Comments.

Table 3. Performance of a GBDT model trained on a downstream task on data generated by different tabular generative models (and on real data for comparison). Runs are averaged across 5 synthetic datasets and 10 GBDT training runs. Dashes denote results worse than the optimal constant solution.

	Method	ABAL ( $R^2$ )	ADUL ( $F_1$ )	BUDD ( $F_1$ )	CALI ( $R^2$ )	CARD ( $F_1$ )	CHUR ( $F_1$ )	DIAB ( $F_1$ )
0	Real	0.556 $\pm$ 0.004	0.815 $\pm$ 0.002	<b>0.906</b> $\pm$ 0.002	0.857 $\pm$ 0.001	0.738 $\pm$ 0.001	0.740 $\pm$ 0.009	0.785 $\pm$ 0.013
1	DiSK	<b>0.550</b> $\pm$ 0.009	<b>0.800</b> $\pm$ 0.002	<b>0.907</b> $\pm$ 0.003	<b>0.842</b> $\pm$ 0.002	<b>0.736</b> $\pm$ 0.001	<b>0.742</b> $\pm$ 0.006	<b>0.763</b> $\pm$ 0.016
2	TDDPM	<b>0.550</b> $\pm$ 0.010	0.795 $\pm$ 0.001	<b>0.906</b> $\pm$ 0.003	0.836 $\pm$ 0.002	<b>0.737</b> $\pm$ 0.001	<b>0.755</b> $\pm$ 0.006	0.740 $\pm$ 0.020
3	SMOTE	<b>0.549</b> $\pm$ 0.005	0.791 $\pm$ 0.002	0.891 $\pm$ 0.003	<b>0.840</b> $\pm$ 0.001	0.732 $\pm$ 0.001	<b>0.743</b> $\pm$ 0.005	0.683 $\pm$ 0.037
4	CTAB-GAN+	0.467 $\pm$ 0.004	0.772 $\pm$ 0.003	0.884 $\pm$ 0.005	0.525 $\pm$ 0.004	0.733 $\pm$ 0.001	0.702 $\pm$ 0.012	0.734 $\pm$ 0.020
5	CTAB-GAN	–	0.783 $\pm$ 0.002	0.855 $\pm$ 0.005	–	0.717 $\pm$ 0.001	0.688 $\pm$ 0.006	0.731 $\pm$ 0.022
6	TVAE	0.433 $\pm$ 0.008	0.781 $\pm$ 0.002	0.864 $\pm$ 0.005	0.752 $\pm$ 0.001	0.717 $\pm$ 0.001	0.732 $\pm$ 0.006	0.714 $\pm$ 0.039
	FB-C ( $R^2$ )	GEST ( $F_1$ )	HIGG ( $F_1$ )	HOUS ( $R^2$ )	INSU ( $R^2$ )	KING ( $R^2$ )	MINI ( $F_1$ )	WILT ( $F_1$ )
0	0.837 $\pm$ 0.001	0.636 $\pm$ 0.007	0.724 $\pm$ 0.001	0.662 $\pm$ 0.003	0.814 $\pm$ 0.001	0.907 $\pm$ 0.002	0.934 $\pm$ 0.000	0.898 $\pm$ 0.006
1	0.687 $\pm$ 0.004	0.605 $\pm$ 0.008	<b>0.721</b> $\pm$ 0.001	0.624 $\pm$ 0.005	<b>0.820</b> $\pm$ 0.003	<b>0.876</b> $\pm$ 0.006	0.926 $\pm$ 0.001	<b>0.892</b> $\pm$ 0.007
2	0.713 $\pm$ 0.002	0.597 $\pm$ 0.006	<b>0.722</b> $\pm$ 0.001	<b>0.677</b> $\pm$ 0.010	0.809 $\pm$ 0.002	0.833 $\pm$ 0.014	<b>0.936</b> $\pm$ 0.001	<b>0.904</b> $\pm$ 0.009
3	<b>0.803</b> $\pm$ 0.002	<b>0.658</b> $\pm$ 0.007	<b>0.722</b> $\pm$ 0.001	0.662 $\pm$ 0.004	<b>0.812</b> $\pm$ 0.002	0.842 $\pm$ 0.004	0.932 $\pm$ 0.001	<b>0.913</b> $\pm$ 0.007
4	0.509 $\pm$ 0.011	0.406 $\pm$ 0.009	0.664 $\pm$ 0.002	0.504 $\pm$ 0.005	0.797 $\pm$ 0.005	0.444 $\pm$ 0.014	0.892 $\pm$ 0.002	0.798 $\pm$ 0.021
5	–	0.392 $\pm$ 0.006	0.575 $\pm$ 0.004	–	–	–	0.889 $\pm$ 0.002	0.906 $\pm$ 0.019
6	0.685 $\pm$ 0.003	0.434 $\pm$ 0.006	0.638 $\pm$ 0.003	0.493 $\pm$ 0.006	0.784 $\pm$ 0.010	0.824 $\pm$ 0.003	0.912 $\pm$ 0.001	0.501 $\pm$ 0.012

## 6. Discussion and future work

In this work, we propose DiSK, an architecture and training paradigm with a good inductive bias for structured data. We show applications of our approach to modeling entities with heterogeneous data types and achieve state-of-the-art generative and predictive quality in most settings. In particular, we show good results generating synthetic, heterogeneous tabular data and numerical predictions. This requires good handling of numerical values which we achieve through our tokenization-free handling via GMMs. The probabilistic nature of the model and its high-precision predictions for numerical types make it suitable for a range of tasks. Another strong appeal is that DiSK both produces and operates on explicitly human-interpretable structured data means that the learnt knowledge in this setting is amenable to both human inspection and curation.

This architecture and the corresponding training approach present a step towards our broader research vision of enabling better reasoning and knowledge manipulation. From our experiments with LLaMA, it is evident that Language Models fall short when used as knowledge stores, underscoring the need for an approach which offers a more effective method for reasoning about structured entities in knowledge bases. Integrating DiSK with language models promises improvements in such tasks, but requires exploration especially in leveraging relationships within knowledge graphs for better generalization (see Appendix G for limitations).

Future work will explore jointly training a combination of DiSK and an LLM for tasks like structured entity extraction from text and KB-augmented text generation. Unlike KB

completion, for structured entity extraction DiSK would need to predict the entity properties based on LLM’s latent representation of text, rather than unmasked properties. For KB-augmented text generation tasks, such as question-answering, it is the LLM that may attend over the latent representations of entities and properties from DiSK. The ability to employ the same DiSK model to these varied tasks opens up the opportunity to explore large-scale multitask pre-training of DiSK, a potential stepping stone towards foundation models of structured entities and KBs. While large-scale KBs with structured entities are already available for pre-training, the ability to extract more structured information from text (and other modalities) creates a virtuous cycle by producing more data that may be employed for the training of DiSK.

## Impact Statement

This paper presents work whose goal is to advance the field of Machine Learning. There are many potential societal consequences of our work, none which we feel must be specifically highlighted here.

## References

- Allen-Zhu, Z. and Li, Y. Physics of language models: Part 3.2, knowledge manipulation. [arXiv preprint arXiv:2309.14402](https://arxiv.org/abs/2309.14402), 2023.
- Austin, J., Johnson, D. D., Ho, J., Tarlow, D., and Van Den Berg, R. Structured denoising diffusion models in discrete state-spaces. [Advances in Neural Information](https://arxiv.org/abs/2309.14402)



- Processing Systems, 34, 2021.
- Berglund, L., Tong, M., Kaufmann, M., Balesni, M., Stickland, A. C., Korbak, T., and Evans, O. The reversal curse: Lms trained on” a is b” fail to learn” b is a”. arXiv preprint arXiv:2309.12288, 2023.
- Bordes, A., Usunier, N., Garcia-Duran, A., Weston, J., and Yakhnenko, O. Translating embeddings for modeling multi-relational data. Advances in Neural Information Processing Systems, 26, 2013.
- Brown, B. A. Neutron radii in nuclei and the neutron equation of state. Phys. Rev. Lett., 85, 2000.
- Burbidge, M. E., Burbidge, G. R., Fowler, W. A., and Hoyle, F. Synthesis of the elements in stars. Rev. Mod. Phys., 29, 1957.
- Campbell, A., Benton, J., De Bortoli, V., Rainforth, T., Deligiannidis, G., and Doucet, A. A continuous time framework for discrete denoising models. Advances in Neural Information Processing Systems, 35, 2022.
- Chawla, N. V., Bowyer, K. W., Hall, L. O., and Kegelmeyer, W. P. Smote: Synthetic minority over-sampling technique. J. Artif. Int. Res., 16, 2002.
- Devlin, J., Chang, M.-W., Lee, K., and Toutanova, K. BERT: Pre-training of deep bidirectional transformers for language understanding. Proceedings of the 2019 Conference of the North American Chapter of the Association for Computational Linguistics: Human Language Technologies, Volume 1 (Long and Short Papers), June 2019.
- Erler, J., Birge, N., Kortelainen, M., Nazarewicz, W., Olsen, E., Perhac, A., and Stoitsov, M. V. The limits of the nuclear landscape. Nature, 486, 2012.
- Gandolfi, S., Carlson, J., and Reddy, S. The maximum mass and radius of neutron stars and the nuclear symmetry energy. Phys. Rev. C, 85, 2012.
- Gao, Z., Wang, Y., Lü, H., Li, Q., Shen, C., and Liu, L. Machine learning the nuclear mass, 2021.
- Ghazvininejad, M., Levy, O., Liu, Y., and Zettlemoyer, L. Mask-predict: Parallel decoding of conditional masked language models. Proceedings of the 2019 Conference on Empirical Methods in Natural Language Processing and the 9th International Joint Conference on Natural Language Processing (EMNLP-IJCNLP), 2019.
- Horowitz, C. J. and Piekarewicz, J. Neutron star structure and the neutron radius of Pb-208. Phys. Rev. Lett., 86, 2001.
- Hu, E. J., Shen, Y., Wallis, P., Allen-Zhu, Z., Li, Y., Wang, S., Wang, L., and Chen, W. LoRA: Low-rank adaptation of large language models. International Conference on Learning Representations, 2022.
- Kingma, D., Salimans, T., Poole, B., and Ho, J. Variational diffusion models. Advances in neural information processing systems, 34, 2021.
- Kotelnikov, A., Baranchuk, D., Rubachev, I., and Babenko, A. Tabddpm: Modelling tabular data with diffusion models. International Conference on Machine Learning, 2023.
- Lee, C., Kim, J., and Park, N. Codi: Co-evolving contrastive diffusion models for mixed-type tabular synthesis. arXiv preprint arXiv:2304.12654, 2023.
- Li, Y., Bubeck, S., Eldan, R., Del Giorno, A., Gunasekar, S., and Lee, Y. T. Textbooks are all you need ii: phi-1.5 technical report. arXiv preprint arXiv:2309.05463, 2023.
- Lin, Y., Liu, Z., Sun, M., Liu, Y., and Zhu, X. Learning entity and relation embeddings for knowledge graph completion. Proceedings of the AAAI Conference on Artificial Intelligence, 29(1), Feb. 2015. doi: 10.1609/aaai.v29i1.9491.
- Morin, F. and Bengio, Y. Hierarchical probabilistic neural network language model. International Conference on Artificial Intelligence and Statistics, 2005.
- Mu, J., Li, X. L., and Goodman, N. Learning to compress prompts with gist tokens. In Thirty-seventh Conference on Neural Information Processing Systems, 2023. URL <https://openreview.net/forum?id=2DtxPCL3T5>.
- Nathani, D., Chauhan, J., Sharma, C., and Kaul, M. Learning attention-based embeddings for relation prediction in knowledge graphs. Proceedings of the 57th Annual Meeting of the Association for Computational Linguistics, July 2019.
- Oh Song, H., Xiang, Y., Jegelka, S., and Savarese, S. Deep metric learning via lifted structured feature embedding. Proceedings of the IEEE conference on computer vision and pattern recognition, 29, 2016.
- Oord, A. v. d., Li, Y., and Vinyals, O. Representation learning with contrastive predictive coding. arXiv preprint arXiv:1807.03748, 2018.
- Schlichtkrull, M., Kipf, T. N., Bloem, P., Van Den Berg, R., Titov, I., and Welling, M. Modeling relational data with graph convolutional networks. The Semantic Web: 15th International Conference, ESWC 2018, Heraklion, Crete, Greece, June 3–7, 2018, Proceedings 15, 2018.

- Schroff, F., Kalenichenko, D., and Philbin, J. Facenet: A unified embedding for face recognition and clustering. Proceedings of the IEEE conference on computer vision and pattern recognition, 2015.
- Silver, D., Hubert, T., Schrittwieser, J., Antonoglou, I., Lai, M., Guez, A., Lanctot, M., Sifre, L., Kumaran, D., Graepel, T., et al. Mastering chess and shogi by self-play with a general reinforcement learning algorithm. arXiv preprint arXiv:1712.01815, 2017.
- Sohn, K. Improved deep metric learning with multi-class n-pair loss objective. Advances in Neural Information Processing Systems, 29, 2016.
- Sun, Z., Deng, Z.-H., Nie, J.-Y., and Tang, J. Rotate: Knowledge graph embedding by relational rotation in complex space. International Conference on Learning Representations, 2018.
- Sundararaman, D., Si, S., Subramanian, V., Wang, G., Hazarika, D., and Carin, L. Methods for numeracy-preserving word embeddings. Proceedings of the 2020 Conference on Empirical Methods in Natural Language Processing (EMNLP), November 2020.
- Touvron, H., Martin, L., Stone, K., Albert, P., Almahairi, A., Babaei, Y., Bashlykov, N., Batra, S., Bhargava, P., Bhosale, S., et al. Llama 2: Open foundation and fine-tuned chat models. arXiv preprint arXiv:2307.09288, 2023.
- Trinh, T. H., Wu, Y., Le, Q. V., He, H., and Luong, T. Solving olympiad geometry without human demonstrations. Nature, 625(7995):476–482, 2024.
- Vaswani, A., Shazeer, N., Parmar, N., Uszkoreit, J., Jones, L., Gomez, A. N., Kaiser, Ł., and Polosukhin, I. Attention is all you need. Advances in neural information processing systems, 30, 2017.
- Wang, N., Liu, M., Wu, X., and Meng, J. Surface diffuseness correction in global mass formula. Physics Letters B, 734: 215–219, 2014. ISSN 0370-2693. doi: <https://doi.org/10.1016/j.physletb.2014.05.049>.
- Wang, Z.-A., Pei, J., Liu, Y., and Qiang, Y. Bayesian evaluation of incomplete fission yields. Phys. Rev. Lett., 123.
- Wu, X., Lu, Y., and Zhao, P. Multi-task learning on nuclear masses and separation energies with the kernel ridge regression. Physics Letters B, 834, 2022.
- Xu, L., Skoularidou, M., Cuesta-Infante, A., and Veeramachaneni, K. Modeling tabular data using conditional gan. Advances in Neural Information Processing Systems, 32, 2019.
- Yang, G., Hu, E. J., Babuschkin, I., Sidor, S., Liu, X., Farhi, D., Ryder, N., Pachocki, J., Chen, W., and Gao, J. Tensor programs v: Tuning large neural networks via zero-shot hyperparameter transfer. arXiv preprint arXiv:2203.03466, 2022.
- Zeng, L.-X., Yin, Y.-Y., Dong, X.-X., and Geng, L.-S. Nuclear binding energies in artificial neural networks. arxiv preprint arxiv:2210.02906, 2022.
- Zhao, Y., Gu, A., Varma, R., Luo, L., Huang, C.-C., Xu, M., Wright, L., Shojanazeri, H., Ott, M., Shleifer, S., et al. Pytorch fsdp: experiences on scaling fully sharded data parallel. arXiv preprint arXiv:2304.11277, 2023.
- Zhao, Z., Kunar, A., Birke, R., and Chen, L. Y. Ctab-gan: Effective table data synthesizing. Asian Conference on Machine Learning, 2021.
- Zhu, Z. A. and Li, Y. Physics of language models: Part 3.1, knowledge storage and extraction. arxiv preprint arxiv:2309.14316, 2023.

## A. Diffusion Loss

### A.1. A simple simulation of the reverse process

The general form of the reverse process is as follows

$$\hat{R}_t(\mathbf{x}, \tilde{\mathbf{x}}) = \sum_{d=1}^D \delta(\mathbf{x}^{-d}, \tilde{\mathbf{x}}^{-d}) \hat{R}_t^d(\mathbf{x}, \tilde{x}^d), \quad (6)$$

where

$$\hat{R}_t^d(\mathbf{x}, \tilde{x}^d) = R_t^d(\tilde{x}^d, x^d) \sum_{x_0^d} p_{0|t}^\theta(x_0^d | \mathbf{x}^{-d}) \frac{q_{t|0}(\tilde{x}^d | x_0^d)}{q_{t|0}(x^d | x_0^d)} \quad (7)$$

The term  $\hat{R}_t^d(\mathbf{x}, \tilde{x}^d)$  denotes the rate of events in the  $d$ -th dimension given the current state. Note that if the forward rate from  $\tilde{x}^d$  to  $x^d$  is zero, then the reverse rate from  $x^d$  to  $\tilde{x}^d$  will also be zero. For our setup, events can only occur out of the masking state in the reverse process, and all of the other states are now absorbing. Substituting the above equations for the rate and marginals of the absorbing process, we have

$$\hat{R}_t^d(\mathbf{x}, \tilde{x}^d) = \begin{cases} 0, & x^d \neq 0 \\ \beta(t) \frac{e^{-\gamma(t)}}{1 - e^{-\gamma(t)}} p_{0|t}^\theta(\tilde{x}^d | \mathbf{x}), & x^d = 0, \tilde{x}^d \neq 0 \\ -\beta(t) \frac{e^{-\gamma(t)}}{1 - e^{-\gamma(t)}}, & x^d = \tilde{x}^d = 0. \end{cases} \quad (8)$$

### A.2. Likelihood Bound

The choice of an absorbing state kernel enables a simplified expression for the loss function with which the network can be trained. The general form of the ELBO (up to a constant) given by (Campbell et al., 2022) is

$$\mathcal{L}_{CT} = \mathbb{E}_{t \sim \mathcal{U}(0,1)} q_t(\mathbf{x}) r_t(\tilde{\mathbf{x}} | \mathbf{x}) \left[ \left\{ \sum_{\mathbf{x}' \neq \mathbf{x}} \hat{R}_t(\mathbf{x}, \mathbf{x}') \right\} - Z_t(\mathbf{x}) \log \hat{R}(\tilde{\mathbf{x}}, \mathbf{x}) \right]. \quad (9)$$

The absorbing state setup enables two simplifications to this bound. First, we substitute in the form of  $Z_t$  and  $\hat{R}_t$  to obtain

$$\mathcal{L}_{CT} = \mathbb{E}_{t \sim \mathcal{U}(0,1)} q_t(\mathbf{x}) r_t(\tilde{\mathbf{x}} | \mathbf{x}) \left[ \left\{ N_t \beta(t) \frac{e^{-\gamma(t)}}{1 - e^{-\gamma(t)}} \right\} - (\beta(t)(N_t - D)) \log \hat{R}(\tilde{\mathbf{x}}, \mathbf{x}) \right]. \quad (10)$$

This substitution has made the first term inside the expectation independent of the state and so omits the need for an additional pass of the neural network. Although Campbell et al. (2022) proposed to use a single pass of the neural net to give a good approximation of the bound, this formulation alleviates the need for that approximation.

Consider now the simulation of  $q_t(\mathbf{x}) r_t(\tilde{\mathbf{x}} | \mathbf{x})$ . Like Campbell et al. (2022) we simulate from the marginal of  $\tilde{\mathbf{x}}$  and analytically marginalize the state  $\mathbf{x}$ . Since we know that in the forward process, all events occur at different times and that each event consists of flipping one property into the mask state (at the same rate across properties), simulating from the marginal  $\psi(\tilde{\mathbf{x}}) = \sum_{\mathbf{x}} q_t(\mathbf{x}) r_t(\tilde{\mathbf{x}} | \mathbf{x})$  can be done by first masking out each property independently with probability  $1 - \exp(-\gamma(t))$ , and then masking out one additional property at random. In the case where all properties become masked by chance, we ignore this sample because  $Z_t = 0$ .

Having sampled from this marginal, consider the conditional state distribution  $q_t(\mathbf{x} | \tilde{\mathbf{x}})$  the state  $\mathbf{x}$  must have exactly one less mask than the state  $\tilde{\mathbf{x}}$ , uniformly at random. So analytically marginalizing this state leads to:

$$\mathcal{L}_{CT} = \mathbb{E}_{t \sim \mathcal{U}(0,1)} \psi(\tilde{\mathbf{x}}) q_t(\mathbf{x} | \tilde{\mathbf{x}}) \left[ \left\{ N_t \beta(t) \frac{e^{-\gamma(t)}}{1 - e^{-\gamma(t)}} \right\} - (\beta(t)(N_t - D)) \log \hat{R}(\tilde{\mathbf{x}}, \mathbf{x}) \right] \quad (11)$$

$$= \mathbb{E}_{t \sim \mathcal{U}(0,1)} \psi(\tilde{\mathbf{x}}) \left[ \left\{ N_t \beta(t) \frac{e^{-\gamma(t)}}{1 - e^{-\gamma(t)}} \right\} - \frac{\beta(t)(N_t - D)}{N_t + 1} \sum_{d | \tilde{x}^d = 0} \log \hat{R}(\tilde{\mathbf{x}}, x^d) \right]. \quad (12)$$

Note that sample  $\tilde{\mathbf{x}}$  has  $N_t + 1$  masked dimensions. We can now make our final substitution using equation 8 to get

$$\mathcal{L}_{CT} = \mathbb{E}_{t \sim \mathcal{U}(0,1)\psi(\tilde{\mathbf{x}})} \left[ \left\{ N_t \beta(t) \frac{e^{-\gamma(t)}}{1 - e^{-\gamma(t)}} \right\} - \frac{\beta(t)(N_t - D)}{N_t + 1} \sum_{d|\tilde{x}^d=0} \log \beta(t) \frac{e^{-\gamma(t)}}{1 - e^{-\gamma(t)}} p_{0|t}^\theta(\tilde{x}^d | \mathbf{x}) \right]. \quad (13)$$

Dropping terms that do not depend on neural network parameters we obtain

$$\mathcal{L}_{CT} = \mathbb{E}_{t \sim \mathcal{U}(0,1)\psi(\tilde{\mathbf{x}})} \left[ -\frac{\beta(t)(N_t - D)}{N_t + 1} \sum_{d|\tilde{x}^d=0} \log p_{0|t}^\theta(\tilde{x}^d | \mathbf{x}) + \text{const} \right]. \quad (14)$$

Finally, we can change the variable of integration from  $t$  to the probability of flipping a property in to the mask state. Writing  $\pi(t) = 1 - \exp(-\gamma(t))$ , we have

$$\frac{d\pi}{dt} = \frac{d\gamma}{dt} e^{-\gamma(t)} = \beta(t)(1 - \pi(t)), \quad (15)$$

and so the objective becomes

$$\mathcal{L}_{CT} = \mathbb{E}_{\pi \sim \mathcal{U}(0,1)\psi(\tilde{\mathbf{x}})} \left[ \frac{1 - \hat{\pi}}{1 - \pi} \frac{D}{N_t + 1} \sum_{d|\tilde{x}^d=0} \log p_{0|t}^\theta(\tilde{x}^d | \mathbf{x}) + \text{const} \right], \quad (16)$$

where we use  $\hat{\pi} = N_t/D$  as the empirical masking rate.

This final simplification of the objective reveals a close connection to self-supervised learning: we have the standard reconstruction loss for randomly masked elements in  $x_0$ , but with a random amount of masking. The factor  $(1 - \hat{\pi})/(1 - \pi)$  is the ratio of non-masked elements to the expected non-masked elements, so will downweight gradients where the amount of information is less than expected i.e., if by chance, more masked are flipped than  $\pi$  would imply, then the sample is down-weighted.

## B. Ablations

### B.1. Autoregressive Diffusion vs. Masked modeling

#### B.1.1. QUANTITATIVE EXAMPLES

Here, we show how our prescription for generating samples from our autoregressive diffusion process compares against simple masked modeling where all masked properties are predicted simultaneously. We show a few qualitative examples, including visually inspecting generated MNIST samples (Appendix B.1.2). In this section, we will make this intuition more quantitative by using our tabular datasets testbed.

We use the same model trained with a random masking rate to generate samples using each approach on each dataset. Then we compare the performance of a downstream model trained on these synthetic samples. The results are shown in Table 4. Unsurprisingly, diffusion-based sampling outperforms masked modeling in all cases. We conjecture the wide variance across tasks in the non-diffusion case to the importance of correlations across features in each dataset. Indeed, if the properties are completely independent, it suffices to sample from the marginals, of which the non-autoregressive model is perfectly capable. However, if there are strong correlations, sampling from the marginals can lead to completely smoothed-out samples, which results in performance no better than a constant baseline.

#### B.1.2. QUALITATIVE EXAMPLES

For a more visual representation of our generative model we train a simple U-Net to generate MNIST images starting from a blank image (fully masked) using an implementation of the reverse process from Appendix A.1. Here we show a few examples conditioned on the digit label.

Binary MNIST images are generated by treating pixels as binary categorical variables and diffusing through pixel space one at a time. As Figure 6 illustrates, diffusion generates coherent sample digits emerging through gradual reveals. In contrast,

**DiSK: A Diffusion Model for Structured Knowledge**

Method	ABAL ( $R^2$ )	ADUL ( $F_1$ )	BUDD ( $F_1$ )	CALI ( $R^2$ )	CARD ( $F_1$ )	CHUR ( $F_1$ )	DIAB ( $F_1$ )
0 Real	0.556 $\pm$ 0.004	0.815 $\pm$ 0.002	0.906 $\pm$ 0.002	0.857 $\pm$ 0.001	0.738 $\pm$ 0.001	0.740 $\pm$ 0.009	0.785 $\pm$ 0.013
1 DiSK	<b>0.550<math>\pm</math>0.009</b>	<b>0.800<math>\pm</math>0.002</b>	<b>0.907<math>\pm</math>0.003</b>	<b>0.842<math>\pm</math>0.002</b>	<b>0.736<math>\pm</math>0.001</b>	<b>0.742<math>\pm</math>0.006</b>	<b>0.763<math>\pm</math>0.016</b>
2 Single-step DiSK	0.027 $\pm$ 0.041	0.776 $\pm$ 0.006	–	0.001 $\pm$ 0.003	0.730 $\pm$ 0.001	0.711 $\pm$ 0.005	0.730 $\pm$ 0.021

---

Method	FB-C ( $R^2$ )	GEST ( $F_1$ )	HIGG ( $F_1$ )	HOUS ( $R^2$ )	INSU ( $R^2$ )	KING ( $R^2$ )	MINI ( $F_1$ )	WILT ( $F_1$ )
0	0.837 $\pm$ 0.001	0.636 $\pm$ 0.007	0.724 $\pm$ 0.001	0.662 $\pm$ 0.003	0.814 $\pm$ 0.001	0.907 $\pm$ 0.002	0.934 $\pm$ 0.000	0.898 $\pm$ 0.006
1	<b>0.687<math>\pm</math>0.004</b>	<b>0.605<math>\pm</math>0.008</b>	<b>0.721<math>\pm</math>0.001</b>	<b>0.624<math>\pm</math>0.005</b>	<b>0.820<math>\pm</math>0.003</b>	<b>0.876<math>\pm</math>0.006</b>	<b>0.926<math>\pm</math>0.001</b>	<b>0.892<math>\pm</math>0.007</b>
2	0.095 $\pm$ 0.025	0.434 $\pm$ 0.009	–	0.002 $\pm$ 0.006	–0.002 $\pm$ 0.013	0.071 $\pm$ 0.050	0.834 $\pm$ 0.002	0.562 $\pm$ 0.031

Table 4. Ablating our autoregressive diffusion (Row 1) against simple masked modeling (Row 2) where all properties are predicted simultaneously.

(non-autoregressive) masked modeling exposes all pixels at once, lacking the proper correlations, evident by the noisy samples. While autoregressive benefits are well-established, this visualization demonstrates that diffusion more accurately captures relationships during entity generation than simple masked modeling.

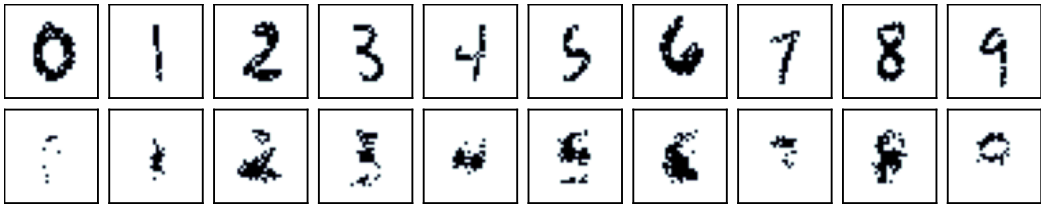


Figure 6. Class-conditioned MNIST samples utilizing (top) a pixel-by-pixel discrete diffusion, or (bottom) unveiling the entire image simultaneously through masked modeling.

Another qualitative example of samples from a DiSK model trained on the GSMarena dataset (see Section 4) highlighting the benefits of this approach in capturing multimodality is shown in Figure 7.

Diffusion Generated {"Manufacturer" : <b>Asus</b> , "Model Name" : Zenfone 2 Laser}	Diffusion Generated {"Manufacturer" : <b>Motorola</b> , "Model Name" : Moto X Play}	Masked Modeling Generated {"Manufacturer" : <b>Motorola</b> , "Model Name" : Zenfone 2 Laser}
---	---	---

Figure 7. Diffusion samples from DiSK yield consistent model names and manufacturers, while masked modeling mismatches manufacturers and names by only capturing marginals.

**B.2. Ablations for prediction quality on GSM**

In this section we run several ablations on different model choices, training on the GSMarena dataset and evaluating with respect to RMS, accuracy and word IOU (compare with Table 1). Overall we find that the models performance is quite stable with respect to the changes we introduce. We include experiments for two different hidden dimensions, two different learning rates, periodic and DICE embeddings, number of GMM mixtures and whether or not numerical embeddings are shared across properties. Table 5 provides the data on all the experiments we ran for this section. We break up interesting aspects into smaller tables 6-8 for better overview. The performance for each setting is averaged over 5 model initialization seeds. In the smaller tables, we highlight the best performance for each property, solely by performance average value, even if multiple models are best within the statistical uncertainty.

**Numerical Embeddings** The first ablation pertains to the treatment of numerical values on the encoder side. Two options are provided for the way in which we embed numerical values, via DICE (Sundaraman et al., 2020) and via periodic embeddings (Vaswani et al., 2017). Additionally, we look at whether tying the embeddings or all nuclear properties has an

effect on performance. We keep other hyperparameters fixed: Notably we run with a model dimension of 512, 50 GMM mixtures for each numerical property, a learning rate of 0.001 and a random mask rate during training. The results are shown in Table 6. They are overall comparable, differences in performance for any field are within one standard deviation. Interestingly, the uncertainty over different initializations seems generally smaller when numerical embeddings are tied.

**GMM vs MSE** In this ablation we vary treatment of numerical properties on the output side. In Figure 5 we illustrate the benefit of using GMMs as opposed to a simple MSE regression, specifically for generation quality. Here, we investigate this choice with respect to prediction quality Experiments are shown in Table 7. The results align with our expectation of similar performance. The reason for this is that in a regression task, we predict the value value as the weighted sum of the mean values of all mixtures, which should attain similar performance as fitting only one Gaussian and predicting its mean.

**Masking rate** During training of a DiSK model, properties are masked out at random. In the scheme derived in Section 3.2 and Appendix A, the rate at which properties are masked is also chosen uniformly at random from 0 to 1. Here, we explore how prediction quality changes when training with a fixed masking rate of 0.5 instead. The results can be seen in Table 8. Interestingly, we seem to find a small but fairly consistent difference in performance. Except for the text field “model”, in which the performance is significantly better, the other predictions are slightly worse when training with the constant masking rate. In future work, we will explore this apparent trade-off further and hope to find how and where the model treats text fields differently than categorical and numerical fields.

num. emb. type	model dim	LR	mask rate (train)	# GMM mixtures	num. emb. tied	weight	height	depth	width	display-size	battery	launch.day	launch.month	launch.year	oem	network-edge	model
dice	256	0.0003	random	1	No	21.797 ± 0.672	6.442 ± 0.099	1.713 ± 0.021	4.158 ± 0.163	0.668 ± 0.024	0.267 ± 0.005	11.528 ± 0.396	3.263 ± 0.018	1.355 ± 0.034	0.227 ± 0.007	0.206 ± 0.003	0.915 ± 0.002
				50	No	21.454 ± 0.222	6.050 ± 0.081	1.712 ± 0.015	3.721 ± 0.063	0.691 ± 0.015	0.247 ± 0.003	11.305 ± 0.363	3.406 ± 0.059	1.394 ± 0.024	0.233 ± 0.008	0.208 ± 0.001	0.915 ± 0.001
				1	Yes	21.323 ± 0.283	6.040 ± 0.077	1.701 ± 0.021	3.608 ± 0.057	0.686 ± 0.009	0.246 ± 0.002	11.195 ± 0.336	3.392 ± 0.024	1.382 ± 0.006	0.207 ± 0.006	0.207 ± 0.003	0.916 ± 0.001
				50	No	22.076 ± 0.595	6.005 ± 0.052	1.688 ± 0.027	3.876 ± 0.111	0.685 ± 0.017	0.239 ± 0.008	11.344 ± 0.192	3.272 ± 0.024	1.272 ± 0.029	0.200 ± 0.002	0.208 ± 0.002	0.908 ± 0.002
				50	No	21.727 ± 0.448	5.770 ± 0.076	1.688 ± 0.011	3.619 ± 0.061	0.663 ± 0.019	0.243 ± 0.002	11.463 ± 0.745	3.371 ± 0.003	1.303 ± 0.028	0.204 ± 0.005	0.210 ± 0.004	0.908 ± 0.001
	512	0.001	random	1	Yes	21.957 ± 0.552	5.725 ± 0.098	1.686 ± 0.014	3.566 ± 0.054	0.652 ± 0.008	0.240 ± 0.003	11.402 ± 0.295	3.370 ± 0.000	1.276 ± 0.025	0.201 ± 0.007	0.210 ± 0.002	0.907 ± 0.002
				50	No	22.082 ± 0.571	5.746 ± 0.167	1.657 ± 0.009	3.577 ± 0.059	0.632 ± 0.016	0.246 ± 0.011	11.165 ± 0.572	3.416 ± 0.049	1.276 ± 0.045	0.183 ± 0.004	0.211 ± 0.003	0.900 ± 0.003
				50	No	21.236 ± 0.465	5.516 ± 0.120	1.612 ± 0.016	3.324 ± 0.058	0.636 ± 0.022	0.236 ± 0.001	11.388 ± 0.837	3.353 ± 0.028	1.258 ± 0.062	0.184 ± 0.007	0.216 ± 0.008	0.901 ± 0.001
				50	Yes	20.711 ± 0.367	5.679 ± 0.119	1.641 ± 0.026	3.298 ± 0.079	0.650 ± 0.008	0.232 ± 0.002	11.204 ± 0.519	3.444 ± 0.025	1.241 ± 0.060	0.180 ± 0.006	0.213 ± 0.004	0.901 ± 0.002
				50	No	22.416 ± 1.105	5.485 ± 0.065	1.789 ± 0.030	3.329 ± 0.268	0.653 ± 0.005	0.241 ± 0.013	11.472 ± 0.473	3.372 ± 0.010	1.341 ± 0.068	0.181 ± 0.007	0.220 ± 0.005	0.883 ± 0.002
Periodic	256	0.0003	random	1	Yes	22.163 ± 0.855	5.719 ± 0.129	1.792 ± 0.041	3.736 ± 0.222	0.628 ± 0.011	0.234 ± 0.005	11.372 ± 0.284	3.369 ± 0.012	1.357 ± 0.095	0.181 ± 0.005	0.233 ± 0.006	0.886 ± 0.002
				50	No	21.801 ± 0.643	6.014 ± 0.128	1.663 ± 0.039	4.004 ± 0.225	0.655 ± 0.018	0.257 ± 0.008	11.158 ± 0.546	3.313 ± 0.017	1.279 ± 0.045	0.204 ± 0.004	0.207 ± 0.005	0.906 ± 0.003
				50	No	21.299 ± 0.553	5.961 ± 0.109	1.686 ± 0.025	3.533 ± 0.083	0.668 ± 0.019	0.242 ± 0.004	11.658 ± 0.533	3.385 ± 0.016	1.299 ± 0.017	0.205 ± 0.005	0.205 ± 0.004	0.907 ± 0.003
				50	Yes	21.006 ± 0.389	5.985 ± 0.172	1.694 ± 0.032	3.517 ± 0.060	0.663 ± 0.016	0.242 ± 0.001	11.326 ± 0.633	3.400 ± 0.051	1.312 ± 0.029	0.205 ± 0.005	0.207 ± 0.007	0.909 ± 0.002
				50	No	22.602 ± 0.726	5.851 ± 0.141	1.683 ± 0.035	3.826 ± 0.090	0.637 ± 0.004	0.251 ± 0.010	11.584 ± 0.594	3.393 ± 0.022	1.280 ± 0.055	0.188 ± 0.004	0.215 ± 0.006	0.894 ± 0.003
	512	0.001	random	1	Yes	21.684 ± 0.432	5.734 ± 0.097	1.714 ± 0.019	3.467 ± 0.067	0.628 ± 0.010	0.237 ± 0.001	11.664 ± 0.513	3.422 ± 0.117	1.245 ± 0.036	0.187 ± 0.003	0.211 ± 0.004	0.894 ± 0.003
				50	Yes	21.551 ± 0.297	5.723 ± 0.098	1.689 ± 0.030	3.453 ± 0.083	0.635 ± 0.016	0.238 ± 0.002	11.316 ± 0.544	3.369 ± 0.002	1.266 ± 0.038	0.189 ± 0.003	0.217 ± 0.005	0.884 ± 0.003
				50	No	23.039 ± 0.565	5.640 ± 0.220	1.686 ± 0.031	3.806 ± 0.475	0.631 ± 0.011	0.252 ± 0.012	11.198 ± 0.273	3.610 ± 0.037	1.260 ± 0.067	0.175 ± 0.002	0.222 ± 0.006	0.880 ± 0.002
				50	No	20.788 ± 0.529	5.648 ± 0.185	1.673 ± 0.045	3.485 ± 0.347	0.637 ± 0.016	0.233 ± 0.008	10.910 ± 0.987	3.351 ± 0.025	1.252 ± 0.057	0.181 ± 0.005	0.230 ± 0.005	0.881 ± 0.004
				50	Yes	20.634 ± 0.480	5.532 ± 0.080	1.689 ± 0.036	3.277 ± 0.063	0.627 ± 0.016	0.243 ± 0.009	11.283 ± 0.176	3.410 ± 0.114	1.268 ± 0.039	0.178 ± 0.005	0.224 ± 0.008	0.880 ± 0.004
Periodic	256	0.0003	random	1	Yes	25.429 ± 1.583	5.861 ± 0.181	1.829 ± 0.028	4.033 ± 0.501	0.657 ± 0.012	0.247 ± 0.013	11.224 ± 0.264	3.934 ± 0.037	1.397 ± 0.068	0.186 ± 0.003	0.237 ± 0.007	0.862 ± 0.004
				50	No	22.611 ± 1.280	5.827 ± 0.090	1.927 ± 0.032	3.594 ± 0.254	0.660 ± 0.024	0.247 ± 0.013	11.124 ± 0.533	3.370 ± 0.014	1.396 ± 0.032	0.186 ± 0.003	0.237 ± 0.007	0.862 ± 0.004
				50	Yes	23.092 ± 0.989	5.894 ± 0.147	1.934 ± 0.046	3.577 ± 0.456	0.685 ± 0.016	0.241 ± 0.007	11.256 ± 0.345	3.358 ± 0.025	1.443 ± 0.064	0.182 ± 0.003	0.232 ± 0.006	0.861 ± 0.002
				50	No	21.496 ± 1.298	6.817 ± 0.300	1.730 ± 0.024	4.344 ± 0.999	0.709 ± 0.023	0.258 ± 0.008	11.810 ± 0.493	3.285 ± 0.010	1.396 ± 0.020	0.238 ± 0.003	0.215 ± 0.006	0.919 ± 0.003
				50	No	21.386 ± 0.756	6.336 ± 0.178	1.798 ± 0.044	3.868 ± 0.089	0.710 ± 0.013	0.249 ± 0.003	11.292 ± 0.487	3.383 ± 0.022	1.465 ± 0.024	0.239 ± 0.003	0.211 ± 0.005	0.917 ± 0.001
	512	0.5	random	1	Yes	21.548 ± 0.984	6.658 ± 0.253	1.775 ± 0.050	3.909 ± 0.077	0.722 ± 0.013	0.240 ± 0.003	11.349 ± 0.270	3.381 ± 0.024	1.459 ± 0.033	0.236 ± 0.006	0.216 ± 0.007	0.917 ± 0.001
				50	No	22.122 ± 0.748	5.830 ± 0.039	1.726 ± 0.013	3.786 ± 0.086	0.674 ± 0.012	0.246 ± 0.002	11.807 ± 0.283	3.302 ± 0.028	1.319 ± 0.017	0.205 ± 0.005	0.212 ± 0.003	0.910 ± 0.002
				50	No	22.122 ± 0.748	5.830 ± 0.039	1.726 ± 0.013	3.786 ± 0.086	0.674 ± 0.012	0.246 ± 0.002	11.807 ± 0.283	3.302 ± 0.028	1.319 ± 0.017	0.205 ± 0.005	0.212 ± 0.003	0.910 ± 0.002
				50	Yes	22.133 ± 0.810	5.949 ± 0.071	1.745 ± 0.027	3.804 ± 0.157	0.672 ± 0.013	0.244 ± 0.003	11.645 ± 0.264	3.381 ± 0.021	1.339 ± 0.017	0.207 ± 0.008	0.215 ± 0.007	0.910 ± 0.001
				50	No	21.989 ± 0.934	5.851 ± 0.225	1.652 ± 0.039	3.817 ± 0.247	0.652 ± 0.025	0.245 ± 0.008	11.523 ± 0.357	3.421 ± 0.049	1.259 ± 0.032	0.182 ± 0.004	0.210 ± 0.004	0.902 ± 0.001
Periodic	256	0.0003	random	1	Yes	21.567 ± 0.590	5.538 ± 0.158	1.686 ± 0.041	3.532 ± 0.121	0.649 ± 0.023	0.237 ± 0.003	11.400 ± 0.491	3.334 ± 0.033	1.275 ± 0.039	0.188 ± 0.004	0.217 ± 0.009	0.903 ± 0.003
				50	Yes	24.006 ± 2.138	5.924 ± 0.314	1.727 ± 0.025	4.006 ± 0.554	0.648 ± 0.029	0.250 ± 0.015	11.367 ± 0.377	3.707 ± 0.052	1.353 ± 0.060	0.183 ± 0.003	0.235 ± 0.007	0.886 ± 0.004
				50	No	22.254 ± 0.479	5.827 ± 0.377	1.844 ± 0.043	3.603 ± 0.135	0.654 ± 0.017	0.243 ± 0.005	11.243 ± 0.252	3.354 ± 0.021	1.435 ± 0.035	0.185 ± 0.009	0.235 ± 0.004	0.888 ± 0.004
				50	Yes	22.380 ± 0.421	5.677 ± 0.252	1.806 ± 0.021	3.739 ± 0.453	0.669 ± 0.030	0.240 ± 0.008	11.347 ± 0.397	3.373 ± 0.014	1.376 ± 0.052	0.187 ± 0.007	0.236 ± 0.009	0.889 ± 0.002
				50	No	22.104 ± 0.948	6.501 ± 0.315	1.715 ± 0.034	4.227 ± 0.218	0.692 ± 0.046	0.258 ± 0.010	11.607 ± 0.340	3.392 ± 0.025	1.316 ± 0.020	0.208 ± 0.004	0.205 ± 0.008	0.908 ± 0.002
	512	0.5	random	1	Yes	20.925 ± 0.459	6.409 ± 0.165	1.752 ± 0.036	3.870 ± 0.145	0.692 ± 0.011	0.245 ± 0.002	11.369 ± 0.142	3.390 ± 0.033	1.406 ± 0.041	0.214 ± 0.002	0.210 ± 0.002	0.912 ± 0.002
				50	Yes	20.551 ± 0.531	6.578 ± 0.388	1.752 ± 0.039	3.849 ± 0.079	0.692 ± 0.008	0.246 ± 0.002	11.366 ± 0.101	3.393 ± 0.021	1.371 ± 0.033	0.211 ± 0.010	0.214 ± 0.002	0.912 ± 0.002
				50	No	23.160 ± 1.348	6.114 ± 0.144	1.711 ± 0.028	4.121 ± 0.116	0.655 ± 0.021	0.247 ± 0.013	11.348 ± 0.285	3.402 ± 0.050	1.281 ± 0.056	0.195 ± 0.007	0.215 ± 0.005	0.899 ± 0.001
				50	No	22.089 ± 0.400	5.993 ± 0.187	1.734 ± 0.024	3.671 ± 0.038	0.659 ± 0.021	0.240 ± 0.004	11.269 ± 0.447	3.371 ± 0.011	1.364 ± 0.032	0.199 ± 0.005	0.219 ± 0.003	0.898 ± 0.004
				50	Yes	22.001 ± 0.629	5.998 ± 0.066	1.744 ± 0.037	3.752 ± 0.073	0.636 ± 0.014	0.239 ± 0.002	11.273 ± 0.300	3.366 ± 0.001	1.308 ± 0.061	0.198 ± 0.005	0.220 ± 0.007	0.898 ± 0.002
Periodic	0.001	random	1	No	23.161 ± 1.593	5.884 ± 0.209	1.740 ± 0.044	3.916 ± 0.318	0.655 ± 0.029	0.256 ± 0.028	11.209 ± 0.713	3.637 ± 0.036	1.277 ± 0.066	0.186 ± 0.003	0.225 ± 0.008	0.883 ± 0.001	
			50	No	22.193 ± 0.910	5.677 ± 0.155	1.712 ± 0.022	3.885 ± 0.461	0.665 ± 0.021	0.240 ± 0.006	11.054 ± 0.529	3.317 ± 0.023	1.317 ± 0.039	0.187 ± 0.008	0.230 ± 0.006	0.882 ± 0.003	
			50	Yes	21.181 ± 0.663	5.618 ± 0.063	1.673 ± 0.030	3.552 ± 0.134	0.633 ± 0.031	0.237 ± 0.008	11.664 ± 0.117	3.375 ± 0.031	1.273 ± 0.032	0.182 ± 0.002	0.228 ± 0.010	0.883 ± 0.002	
			50	No	25.194 ± 2.407	6.157 ± 0.339	1.909 ± 0.093	4.051 ± 0.176	0.677 ± 0.051	0.254 ± 0.022	11.225 ± 0.320	3.369 ± 0.009	1.424 ± 0.045	0.185 ± 0.006	0.235 ± 0.006	0.865 ± 0.002	
			50	No	24.485 ± 1.066	6.372 ± 0.321	1.945 ± 0.058	4.281 ± 0.316	0.714 ± 0.051	0.242 ± 0.004	11.228 ± 0.320	3.369 ± 0.009	1.424 ± 0.045	0.185 ± 0.006	0.236 ± 0.005	0.865 ± 0.002	
50	Yes	23.484 ± 1.710	6.047 ± 0.420	1.904 ± 0.065	4.111 ± 0.546	0.732 ± 0.066	0.248 ± 0.005	11.336 ± 0.165	3.365 ± 0.003	1.398 ± 0.098	0.187 ± 0.007	0.231 ± 0.006	0.866 ± 0.002				

Table 5. Ablations over embedding types, mask rates number of mixtures in the GMMs and tied numerical embeddings.

num. emb. type num. emb. tied	DICE		Periodic Embedding	
	No	Yes	No	Yes
weight	20.788 $\pm$ 0.529	<b>20.634</b> $\pm$ 0.480	22.193 $\pm$ 0.910	21.181 $\pm$ 0.663
height	5.648 $\pm$ 0.185	<b>5.532</b> $\pm$ 0.080	5.677 $\pm$ 0.155	5.618 $\pm$ 0.063
depth	<b>1.673</b> $\pm$ 0.045	1.689 $\pm$ 0.036	1.712 $\pm$ 0.022	1.673 $\pm$ 0.030
width	3.485 $\pm$ 0.347	<b>3.277</b> $\pm$ 0.063	3.885 $\pm$ 0.461	3.552 $\pm$ 0.134
display-size	0.637 $\pm$ 0.016	<b>0.627</b> $\pm$ 0.016	0.665 $\pm$ 0.023	0.633 $\pm$ 0.031
battery	<b>0.233</b> $\pm$ 0.008	0.243 $\pm$ 0.009	0.240 $\pm$ 0.008	0.237 $\pm$ 0.006
launch.day	<b>10.910</b> $\pm$ 0.987	11.283 $\pm$ 0.176	11.054 $\pm$ 0.529	11.664 $\pm$ 0.117
launch.month	3.351 $\pm$ 0.025	3.410 $\pm$ 0.114	<b>3.317</b> $\pm$ 0.023	3.375 $\pm$ 0.031
launch.year	<b>1.252</b> $\pm$ 0.057	1.268 $\pm$ 0.039	1.316 $\pm$ 0.039	1.273 $\pm$ 0.032
oem	0.181 $\pm$ 0.005	<b>0.178</b> $\pm$ 0.005	0.187 $\pm$ 0.008	0.182 $\pm$ 0.002
network-edge	0.230 $\pm$ 0.005	<b>0.224</b> $\pm$ 0.008	0.230 $\pm$ 0.006	0.228 $\pm$ 0.010
model	0.881 $\pm$ 0.004	<b>0.880</b> $\pm$ 0.004	0.882 $\pm$ 0.003	0.883 $\pm$ 0.002

Table 6. Property prediction performance of the DiSK on the GSM dataset, with two different numerical embeddings, either tied or untied. In the tied case, the numerical embeddings are shared between all numerical properties. Runs are averaged over 5 model initialization seeds. Other hyperparameters are fixed.

num. emb. type # GMM mixtures	DICE		Periodic Embedding	
	1	50	1	50
weight	23.039 $\pm$ 0.565	<b>20.788</b> $\pm$ 0.529	23.161 $\pm$ 1.593	22.193 $\pm$ 0.910
height	<b>5.640</b> $\pm$ 0.220	5.648 $\pm$ 0.185	5.884 $\pm$ 0.209	5.677 $\pm$ 0.155
depth	1.686 $\pm$ 0.031	<b>1.673</b> $\pm$ 0.045	1.740 $\pm$ 0.044	1.712 $\pm$ 0.022
width	3.806 $\pm$ 0.475	<b>3.485</b> $\pm$ 0.347	3.916 $\pm$ 0.318	3.885 $\pm$ 0.461
display-size	<b>0.631</b> $\pm$ 0.011	0.637 $\pm$ 0.016	0.655 $\pm$ 0.029	0.665 $\pm$ 0.023
battery	0.252 $\pm$ 0.012	<b>0.233</b> $\pm$ 0.008	0.256 $\pm$ 0.028	0.240 $\pm$ 0.008
launch.day	11.198 $\pm$ 0.273	<b>10.910</b> $\pm$ 0.987	11.209 $\pm$ 0.713	11.054 $\pm$ 0.529
launch.month	3.610 $\pm$ 0.037	3.351 $\pm$ 0.025	3.637 $\pm$ 0.056	<b>3.317</b> $\pm$ 0.023
launch.year	1.260 $\pm$ 0.067	<b>1.252</b> $\pm$ 0.057	1.277 $\pm$ 0.066	1.316 $\pm$ 0.039
oem	<b>0.175</b> $\pm$ 0.002	0.181 $\pm$ 0.005	0.186 $\pm$ 0.003	0.187 $\pm$ 0.008
network-edge	<b>0.222</b> $\pm$ 0.006	0.230 $\pm$ 0.005	0.225 $\pm$ 0.008	0.230 $\pm$ 0.006
model	<b>0.880</b> $\pm$ 0.002	0.881 $\pm$ 0.004	0.883 $\pm$ 0.001	0.882 $\pm$ 0.003

Table 7. Prediction performance on GSM with either 1 or 50 GMM mixtures per numerical property. When the number of GMM mixtures is 1, the task reduces to regression via MSE.



num. emb. tied mask rate (training)	No		Yes	
	Random	0.5	Random	0.5
weight	20.788 $\pm$ 0.529	22.611 $\pm$ 1.280	<b>20.634<math>\pm</math>0.480</b>	23.092 $\pm$ 0.989
height	5.648 $\pm$ 0.185	5.827 $\pm$ 0.090	<b>5.532<math>\pm</math>0.080</b>	5.894 $\pm$ 0.147
depth	<b>1.673<math>\pm</math>0.045</b>	1.927 $\pm$ 0.032	1.689 $\pm$ 0.036	1.934 $\pm$ 0.046
width	3.485 $\pm$ 0.347	3.594 $\pm$ 0.254	<b>3.277<math>\pm</math>0.063</b>	3.577 $\pm$ 0.456
display-size	0.637 $\pm$ 0.016	0.660 $\pm$ 0.024	<b>0.627<math>\pm</math>0.016</b>	0.685 $\pm$ 0.016
battery	<b>0.233<math>\pm</math>0.008</b>	0.247 $\pm$ 0.013	0.243 $\pm$ 0.009	0.241 $\pm$ 0.007
launch.day	<b>10.910<math>\pm</math>0.987</b>	11.122 $\pm$ 0.533	11.283 $\pm$ 0.176	11.256 $\pm$ 0.345
launch.month	<b>3.351<math>\pm</math>0.025</b>	3.370 $\pm$ 0.014	3.410 $\pm$ 0.114	3.358 $\pm$ 0.025
launch.year	<b>1.252<math>\pm</math>0.057</b>	1.396 $\pm$ 0.032	1.268 $\pm$ 0.039	1.443 $\pm$ 0.064
oem	0.181 $\pm$ 0.005	0.186 $\pm$ 0.003	<b>0.178<math>\pm</math>0.005</b>	0.182 $\pm$ 0.003
network-edge	0.230 $\pm$ 0.005	0.237 $\pm$ 0.007	<b>0.224<math>\pm</math>0.008</b>	0.232 $\pm$ 0.009
model	0.881 $\pm$ 0.004	0.862 $\pm$ 0.004	0.880 $\pm$ 0.004	<b>0.861<math>\pm</math>0.002</b>

Table 8. Prediction performance on GSM ablated over the mask rate during training. Properties are always masked out randomly, but the probability can be chosen. “Random” means a uniformly random mask rate, newly drawn for each batch. Note that the rate applies only in training.

### C. Architecture and Training Details

Encoders and decoders in the model largely have the same structure, which relies on residual blocks made of a standard  $4\times$  hidden layer, a GLU activation, and a post-activation LayerNorm. Parameters are initialized following the Maximal Update Parameterization (Yang et al., 2022). Categorical decoders have the same number of outputs as classes. Numerical decoders, on the other hand, predict GMM parameters, which add up to a total of  $3 \times \text{Num. Mixtures}$  which is usually a hyperparameter we tune on a validation set. We use the default implementation of the transformer encoder in PyTorch for the entity encoder and the text encoder. Similarly, we use the default transformer decoder for the text decoder. For the text encoder, we use the last layer outputs at the first token as the encoding of the text property. Code for the model architecture, as well as experiments, is available at [github REDACTED].

Preprocessing (for GSMarena and AME2020) includes min-max rescaling for numerical and one-hot encoding for categorical properties. However, we did experiment with semantically encoding the labels of categorical properties using the same tokenization and embeddings from the language modeling component. This yielded interesting results with “semantically meaningful” errors. For instance, if the model never sees a label in the training data, it often predicts a label with a large string intersection with the truth labels. We also experimented with both DICE and trainable periodic embeddings but found no significant difference. Results are reported using periodic embeddings.

We use a cosine annealing schedule for all of our runs. All runs were performed on a handful of V100 GPUs.

The hierarchical encodings are generated by traversing the hierarchy to reach the node for which we would like to compute the prediction (see Figure 9). In our case, we use an RNN to process the sequence and read off the encoding from the hidden representation of the last element in the sequence.

### D. Tabular Datasets Details

**Experimental setup** We use the same experimental setup as (Kotelnikov et al., 2023), including the preprocessing and the CatBoost hyperparameters tuned on the validation set of each dataset. For DiSK, we run a hyperparameter search on learning rate, width, depth, and number of GMM parameters over 100 iterations to optimize the CatBoost performance on the validation set. Finally, we evaluate the test set from the real data after training 10 CatBoost models on 5 realizations of data generated by DiSK, totaling 50 runs. Table 3 reports the mean and the standard deviation. For the other methods, we re-use the hyperparameters reported by (Kotelnikov et al., 2023) and found by tuning each model in a similar fashion.

**Baselines** Our main baseline here is TabDDPM, which is also a diffusion model, though it uses very different assumptions (for instance, a uniform kernel instead of one with an absorbing state). These discrepancies and the differences in architecture enable our approach to be better suited to handling numerical quantities, hierarchical and sparse data, and missing values. We

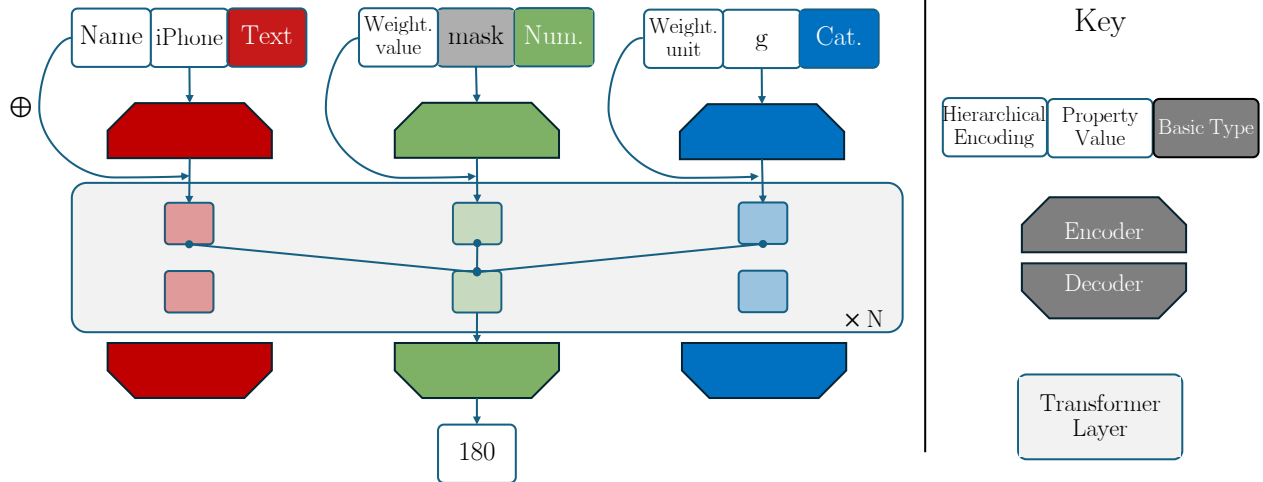


Figure 8. DiSK architecture on the left and key for the diagram on the right. In this example, the model is tasked to predict the masked value for the `weight.value` property.

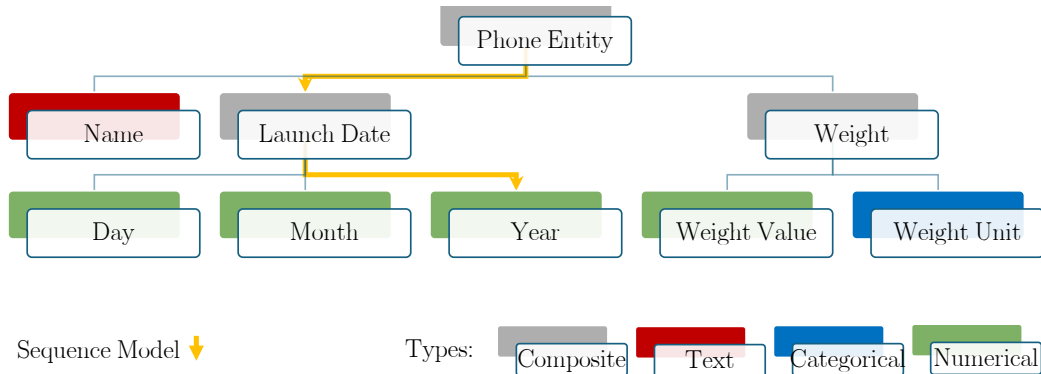


Figure 9. Example phone entity with leaf nodes that have one of the following basic types **numerical**, **categorical**, or **text**. Composite properties are made of other composite types or leaf nodes. Positional encodings are generated at each node using a sequence model over the path that connects it to the root. Encoded values at each node are attended to using the entity encoder

also compare against other generative models: TVAE, a tabular variation auto-encoder-based generative model, CTAB-GAN and its upgrade CTAB-GAN+ based on a generative adversarial backbone. Finally, SMOTE is an interpolation method originally proposed for minority oversampling but is used in (Kotelnikov et al., 2023) as a sanity-check baseline.

**Datasets** Table 9 contains the complete list of the datasets used in this experiment.

### E. Details on nuclear data

The data is gathered from a live chart of nuclide properties in <https://nds.iaea.org/relnsd/vcharthtml/VChartHTML.html> that is constantly updated. Our snapshot includes all data up to August 2023. Sources for the data are listed in <https://nds.iaea.org/relnsd/vcharthtml/guide.html>, subsection *Sources*. This dataset contains numerical and categorical properties. Numerical properties comprise binding energy, charge radius, the logarithm of the half-life, Spin configuration, abundance of the nucleus in nature, energies available for  $\alpha$ ,  $\beta$ ,  $\beta + n$  decays and electron capture (EC), various form factors. The categorical properties are the stability of the nucleus and its parity. We exclude proton/neutron separation energy to prevent binding energy data leakage.

With consistent results across hyperparameter configurations, our chosen model for this task trains for 50,000 epochs with a 0.001 learning rate, no weight decay, 0.1 dropout, and 1024 batch size. It has two encoder/decoder layers per property and 50 GMM components per numerical feature.

Table 9. Dataset description for the experiments on tabular data.

Code	Name	Train size	Val. size	Test size	Num. feat.	Cat. feat.	Task
ABAL	Abalone	2672	669	836	7	1	Regression
ADUL	Adult	26048	6513	16281	6	8	Binclass
BUDD	Buddy	12053	3014	3767	4	5	Multiclass
CALI	California Housing	13209	3303	4128	8	0	Regression
CARD	Cardio	44800	11200	14000	5	6	Binclass
CHUR	Churn Modelling	6400	1600	2000	7	4	Binclass
DIAB	Diabetes	491	123	154	8	0	Binclass
FB-C	Facebook Comments Volume	157638	19722	19720	50	1	Regression
GEST	Gesture Phase	6318	1580	1975	32	0	Multiclass
HIGG	Higgs Small	62751	15688	19610	28	0	Binclass
HOUS	House 16H	14581	3646	4557	16	0	Regression
INSU	Insurance	856	214	268	3	3	Regression
KING	King	13832	3458	4323	17	3	Regression
MINI	MiniBooNE	83240	20811	26013	50	0	Binclass
WILT	Wilt	3096	775	968	5	0	Binclass

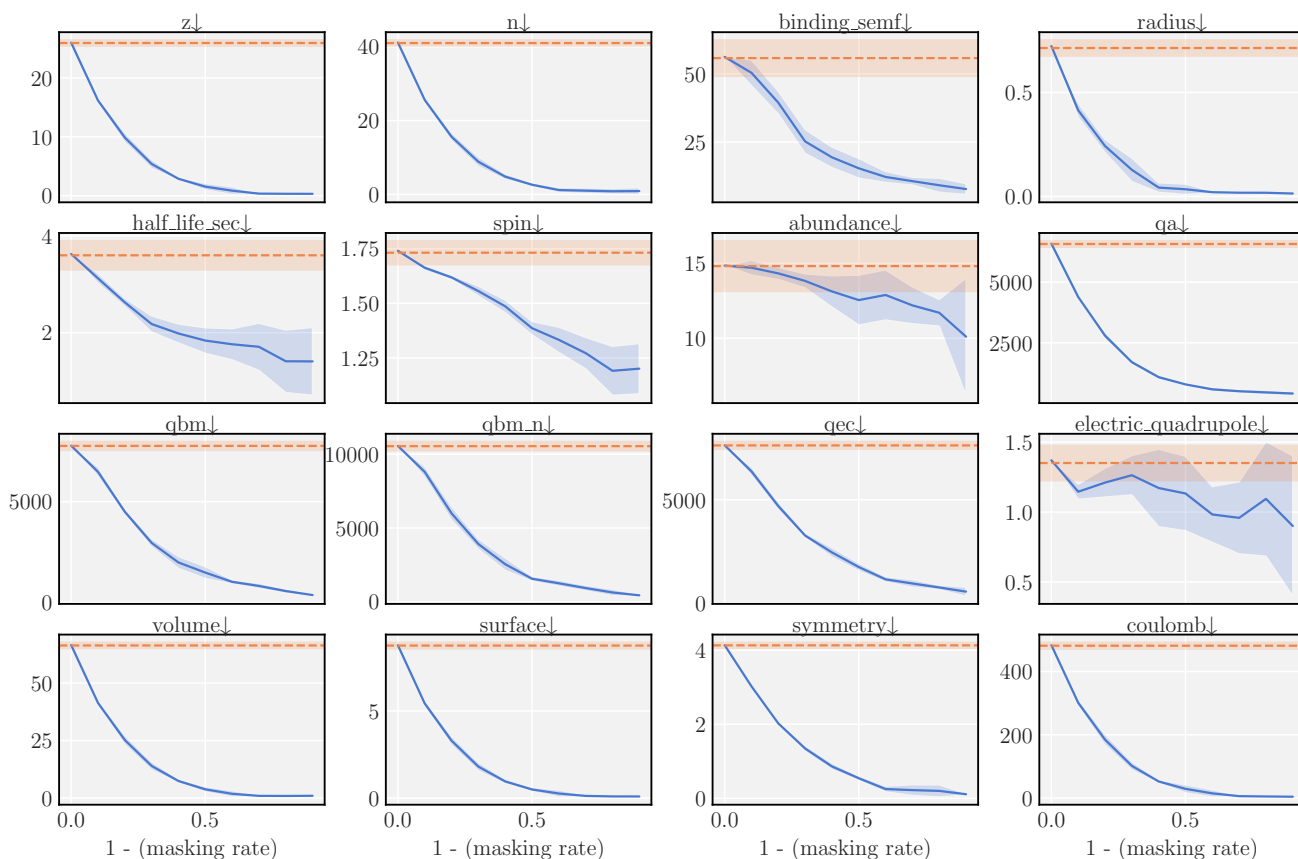


Figure 10. Model performance on a held-out set of the nuclear dataset as a function of masking rate, measured by root mean square error (RMS, ↓) for numerical properties and accuracy (↑) for categorical properties. The dashed baseline reflects always predicting the marginal mode/mean. Error bars are one  $\sigma$ .

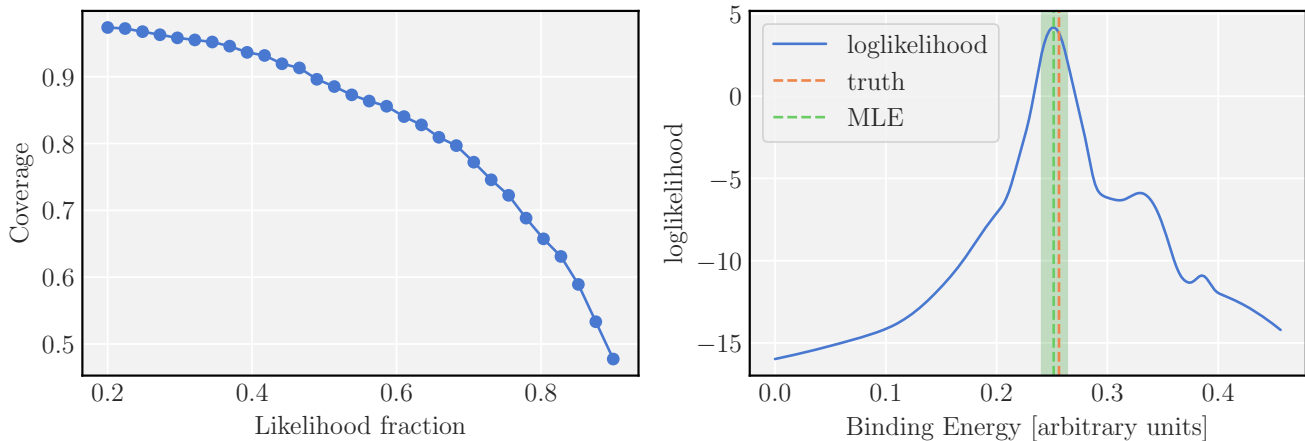


Figure 11. (Left) Coverage of estimated binding energy from the nuclear dataset as a function of maximum loglikelihood fraction contained within the interval. (Right) Full loglikelihood of the binding energy of a validation sample along with the Maximum Likelihood Estimate (MLE) and the  $-1/2$  profile likelihood.

### E.1. Training and Evaluation on Nuclear Data

Evaluating the precision of predictions of Tabular Denoising Diffusion Probabilistic Model (TDDPM) on the nuclear physics dataset requires conditioning on  $N, Z$ . Because this cannot be done directly, we generate samples from the joint distribution which includes  $N$  and  $Z$  and post-hoc condition on samples that are close to the desired  $N$  and  $Z$  values (within 0.1 tolerance). We then take the mean prediction of these samples and use it as a model prediction. We used the standard architecture from Kotelnikov et al. (2023) with slightly different hyperparameters, which were tuned with a validation set on a coarse grid.

As for the GBDT, we handle missing data by filling with the Optimal Constant solution i.e., if a (numerical) categorical property is missing in a particular sample we simply replace it with the (mean) mode of that property across the training set. We chose the following hyperparameters for tuning by suggesting suitable values in each distribution:

1. **learning rate:** The learning rate determines the step size taken by the optimizer during training. We used a log-uniform distribution between 0.001 and 1.0.
2. **depth:** The depth of the decision trees in the model. We chose an integer value between 3 and 10 for this parameter.
3. **l2 leaf reg:** The L2 regularization term applied to the objective function. We used a uniform distribution between 0.1 and 10.0 for this parameter.
4. **bagging temperature:** The parameter controlling the intensity of the sampling process for bagging during training. We used a uniform distribution between 0.0 and 1.0 for this parameter.
5. **leaf estimation iterations:** The number of Newton-Raphson iterations for calculating leaf weights. We chose an integer value between 1 and 10 for this parameter.

Additionally, we set some default values for other parameters:

- iterations: 2000
- early stopping rounds: 50
- od pval: 0.001

### F. Details on the GSM dataset

The GSMarena dataset on phones comes from <https://www.kaggle.com/datasets/msainani/gsmarena-mobile-devices>, comprises 10679 entries of phone entities, with the following features: model

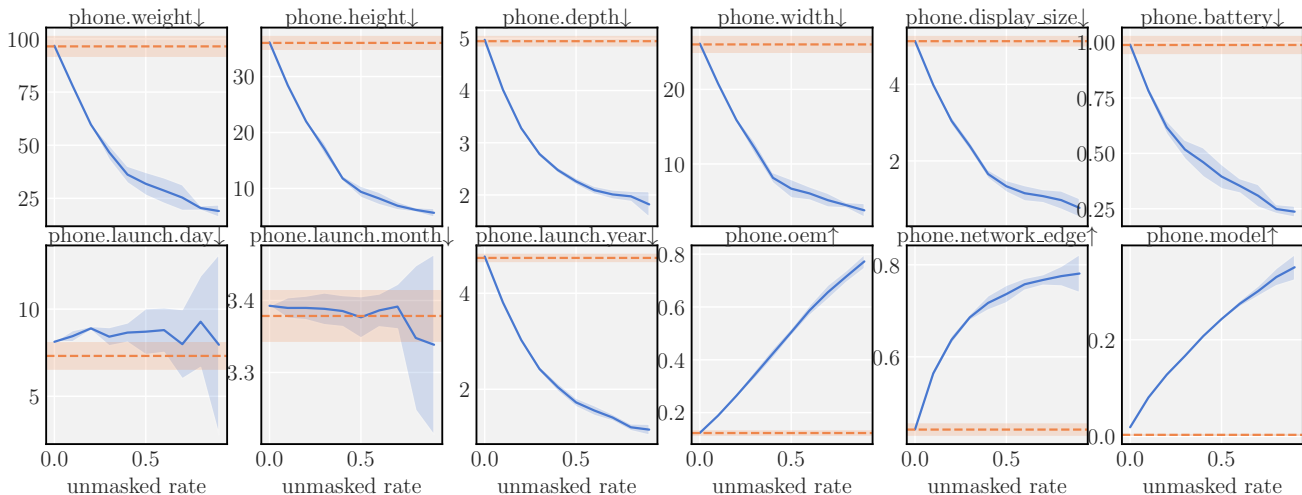


Figure 12. DiSK performance on a held-out dataset as a function of unmasking rate, measured by root mean square error (RMS, ↓) for numerical properties and accuracy (↑) for categorical properties. The dashed baseline reflects always predicting the marginal mode/mean. Error bars are one  $\sigma$ .

name, OEM name, network edge, weight, display size, height, width, depth, battery and launch date, which is a composite type of day, month and year. The data is split into 80% train and 20% test data. A small number of entries shares both the manufacturer and model name. In such cases, we move the duplicates from the testing set to the training set. This results in a split of about 83% and 17%. The phone launch day entry is fairly sparse, only 5% are filled, but all other values have at least 85% coverage.

### E.1. GSM Training for DiSK and Decoder-only

The custom tokenization for the from-scratch trained decoder defines each possible element in categorical fields as one token. Numerical values are represented as floats with two decimals and tokenization is done per digit. The string representation has special tokens for separation between items, key value separation and separation of hierarchical key. For example, a key like `phone.launch.day` is tokenized as “ $T(\text{phone}), T(\cdot), T(\text{launch}), T(\cdot), T(\text{day})$ ”,  $T$  representing the token to integer mapping. The model is a 4-layer decoder-only transformer a model dim of 768, 2 heads per self-attention. It is trained with a batch size of 512, a learning rate of 0.0001, weight decay of 0.0001 and no dropout. Those parameters were optimized by sweeping over a coarse grid.

The DiSK has one encoder and one decoder module with 2 layers each for every feature of the data, a model dimension of 256, 2 heads in each attention, a 2-layer entity encoder and 50 GMM components per feature. It was trained with a batch size of 1024, learning rate of 0.001, no weight decay and a dropout of 0.1 over 20000 epochs. Those parameters were optimized in a similar way as in the decoder procedure.

The Llama model was fine-tuned with LoRA (Hu et al., 2022) and FSDP (Zhao et al., 2023) via the `llama-recipes` repository (<https://github.com/facebookresearch/llama-recipes>) from Meta AI. Training runs for two epochs, after which the validation loss saturates.

### E.2. GSM Training for GBDTs

GBDTs offer state-of-the-art performance on tabular data but they do not handle missing data naturally. To solve this issue, we fill in missing properties with their optimal constant solutions (mean for continuous and mode for discrete). Furthermore, text properties are omitted because GBDTs cannot handle them in a natural fashion. We tune the GBDT hyperparameters on a validation set in a similar way to that of the nuclear physics dataset in Appendix E.1.

## G. Limitations

While our study demonstrates the efficacy of the DiSK model in structured generative modeling and high-precision handling of numerical types along with various data types, several limitations and future research directions emerge:

### 1. Scalability and Pre-training Challenges:

- *Current Scope:* The model’s current application is confined to datasets of a limited scale.
- *Future Aspirations:* Aiming to scale the model to joint training on larger and more varied datasets introduces significant challenges, especially in pre-training.

### 2. Integration with Language Models:

- *Current Integration:* The model has a strong capacity in handling structured data and generating high-precision predictions but uses a small transformer to model text properties.
- *Future Potential:* Extending our approach to integrate with LLMs could enhance performance on knowledge-intensive tasks and benchmarks.

### 3. Generalization within Knowledge Graphs:

- *Current Methodology:* The model treats static entities as independent units, not fully leveraging relational dynamics within a knowledge graph.
- *Future Exploration:* Investigating how the model can achieve generalization within the context of a knowledge graph.

### 4. Knowledge Representation in Foundation Models:

- *Broader Implications:* Current foundation models, including LLMs, store knowledge in latent forms that are not human-interpretable or easily editable.
- *Future Directions:* Developing structured knowledge models to augment LLMs, aiming for explicit, interpretable, and editable knowledge representation, remains an important challenge.